

## Supplementary Information

### Unveiling the impact of photoinduced halide segregation on performance degradation in wide-bandgap perovskite solar cells

Yuxiao Guo,<sup>a</sup> Cong Zhang,<sup>b</sup> Linqin Wang,<sup>c</sup> Xingtian Yin,<sup>b,\*</sup> Bihui Sun,<sup>a</sup> Changting Wei,<sup>a</sup> Xin Luo,<sup>a</sup> Shiyu Yang,<sup>a</sup> Licheng Sun,<sup>c</sup> and Bo Xu<sup>a,\*</sup>

<sup>a</sup> MIIT Key Laboratory of Advanced Display Materials and Devices, School of Materials Science and Engineering, Nanjing University of Science and Technology, Nanjing, Jiangsu 210094, China.

<sup>b</sup> Electronic Materials Research Laboratory, Key Laboratory of the Ministry of Education, International Center for Dielectric Research, Shaanxi Engineering Research Center of Advanced Energy Materials and Devices, School of Electronic Science and Engineering, Xi'an Jiaotong University, Xi'an 710049, Shaanxi, P. R. China.

<sup>c</sup> Center of Artificial Photosynthesis for Solar Fuels and Department of Chemistry, School of Science, Westlake University, Hangzhou 310024, P. R. China

\*Correspondence: xt\_yin@xjtu.edu.cn (X.Y.); boxu@njust.edu.cn (B.X.)

## Experimental Part

### Materials

All chemicals and solvents were used as received without any purification, including nickel oxide nanoparticles ( $\text{NiO}_x$ , 5 ~ 10 nm, Advanced Election Technology, 99.999%), [2-(9H-Carbazol-9-yl)ethyl]phosphonic acid (2PACz, Tokyo Chemical Industry, >98.0%), formamidinium iodide (FAI, Xi'an Yuri Solar, 99.5%), methylammonium iodide (MAI, Xi'an Yuri Solar, 99.5%), methylamine hydrochloride (MACl, Xi'an Yuri Solar, 99.5%), cesium iodide (CsI, Aladdin, 99.9%), lead iodide ( $\text{PbI}_2$ , Aladdin, 99.9%), lead bromide ( $\text{PbBr}_2$ , Aladdin, 99.99%), lead thiocyanate ( $\text{Pb}(\text{SCN})_2$ , Adamas, 98%), 2-phenylethylamine hydroiodide (PEAI, Xi'an Yuri Solar, 99.5%), [6,6]-phenyl-C61-butyric acid methyl ester (PC61BM, Advanced Election Technology, 99.9%), bathocuproine (BCP, Xi'an Yuri Solar, 99%), Molybdenum (VI) oxide ( $\text{MoO}_3$ , Alfa Aesar, 99.9995%), N, N-dimethylformamide (DMF, J&K Scientific, 99.8%), dimethyl sulfoxide (DMSO, J&K Scientific, 99.7%), isopropanol (IPA, Aladdin, ≥99.7%), chlorobenzene (CB, MERYER, 99.8%), and ethyl acetate (EA, Energy Chemical, ≥99.5%). Silver cylinders ( $\phi$  2\*5 mm, 99.99%) were purchased from ZhongNuo New Material (Beijing) Technology Co., Ltd.

### Perovskite deposition

Referring to our previous work,<sup>1</sup>  $\text{FA}_{0.83}\text{Cs}_{0.17}\text{Pb}(\text{I}_{0.6}\text{Br}_{0.4})_3$  precursor with different concentrations of 1.3, 0.975, 0.65, and 0.325 M were obtained by dissolving FAI, CsI,  $\text{PbI}_2$ ,  $\text{PbBr}_2$ , and  $\text{Pb}(\text{SCN})_2$  (1.15 mol%) in mixed solvent of DMF and DMSO (4:1, v/v) and then stirred at 60 °C for 4 hours. Besides, the  $\text{FA}_{0.83}\text{Cs}_{0.17}\text{Pb}(\text{I}_{0.8}\text{Br}_{0.2})_3$  and  $\text{FA}_{0.83}\text{Cs}_{0.17}\text{Pb}(\text{I}_{0.4}\text{Br}_{0.6})_3$  compositions were prepared by adjusting  $\text{PbX}_2$  ratio. Before use, the yellow precursor was filtered twice through 0.45 μm nylon membrane. For film deposition, 70 μL precursor solution was dynamically dispensed onto the substrate

spinning at 1000 rpm, and the substrate was then accelerated to 5000 rpm within 5 seconds and remained at this speed for 25 seconds. 5 seconds before the end of this process, 150  $\mu$ L EA was quickly dropped onto the spinning substrate as an antisolvent quench. Finally, the wet film was directly annealed at 100 °C for 30 minutes.

### Device fabrication

Indium tin oxide glasses (ITO, 15 × 15 mm<sup>2</sup>, ~15  $\Omega$  sq<sup>-1</sup>, South China Science & Technology) were ultrasonically cleaned with deionized water, acetone, and ethanol for 15 minutes, respectively. Before deposition, glass/ITO substrates were dried by compressed air and then treated by UV-ozone for 15 minutes. For HTL deposition, NiO<sub>x</sub> aqueous dispersion (10 mg mL<sup>-1</sup>) was spin-coated onto the substrates at the speed of 2000 rpm, and then annealed at 120 °C for 15 minutes. Then, 2PACz ethanol solution with a concentration of 2 mM were deposited onto NiO<sub>x</sub> layer at 3000 rpm for 30 seconds, followed by annealing at 100 °C for 10 minutes. The substrates were then transferred to a N<sub>2</sub>-filled glovebox for perovskite deposition, according to the above section. After the perovskite films cooled down, the PEAI solution (1 mg mL<sup>-1</sup> in IPA) was spin-coated onto the surface at 4000 rpm for 30 seconds accompanying with an annealing step of 100 °C for 5 minutes. After that, PCBM (20 mg mL<sup>-1</sup> in CB) and BCP (0.5 mg mL<sup>-1</sup> in IPA) layers were prepared with the spinning parameters of 2000 rpm/30 seconds and 5000 rpm/30 seconds, respectively. Finally, 100 nm Ag electrode was thermally evaporated under a vacuum of  $2 \times 10^{-4}$  Pa through the designed mask with an effective area of 0.033 cm<sup>2</sup>.

### Characterization

**Perovskite films.** Absorption spectra was conducted in range from 400 to 800 nm by using a UV-VIS-NIR spectrophotometer (UV-3600, Shimadzu). PL spectra were obtained from a Cary Eclipse Fluorescence spectrophotometer (Agilent Technologies).

Field emission scanning electron microscopy (SEM, GeminiSEM 300, ZEISS) and atomic force microscope (AFM, MultiMode 8, Bruker) were adopted to characterize the surface morphology. A D/max 2400 X Series X-ray diffractometer (XRD, SmartLab, Rigaku) with Cu K $\alpha$ , 1.541 nm radiation (40 kV, 30 mA) was adopted to confirm crystal structure. GIXRD results of samples were conducted by using Rigaku Smartlab 3 kW with an incident angle of 1° and a slow scan rate of 0.5° min<sup>-1</sup> for structure information. PL and lifetime images were obtained through a Leica TCS SP8 STED 3X microscope (Leica, German), in which the excitation source (pulse laser, 470 nm) was focused through an oil immersion objective (100x, NA1.4). TOF-SIMS measurement was performed on a ToF-SIMS.5 instrument, operated in spectral mode using a 30 keV Bi<sup>3+</sup> primary ion beam. For depth profiling, a Cs<sup>+</sup> sputter beam (0.5 keV, 40 nA) was used to remove the material layer-by-layer in interlaced mode from a raster area of 300 × 300 μm<sup>2</sup>. Negative ions were collected for depth profile analysis, and the mass-spectrometry was performed on an area of 100 × 100 μm<sup>2</sup> in the center of sputter crater.

**Devices.** J-V curves between -0.1 and 1.3 V (A scanning rate of 100 mV s<sup>-1</sup>; Dwell time: 20 ms) were obtained by a Keithley 2400 source meter under AM 1.5G illumination, which was provided by a Xenon lamp-based solar simulator (Sirius-SS150A, Zolix). Meanwhile, the steady-state measurements, as well as SCLC testing, were conducted through an electrochemical workstation (DH7000C, Donghua). EL spectra were measured through an integrated LED test system designed by Hamamatsu Photonics Co., Ltd that includes fiber integrated field, Keithley 2400, and PMA-12 spectrometer.

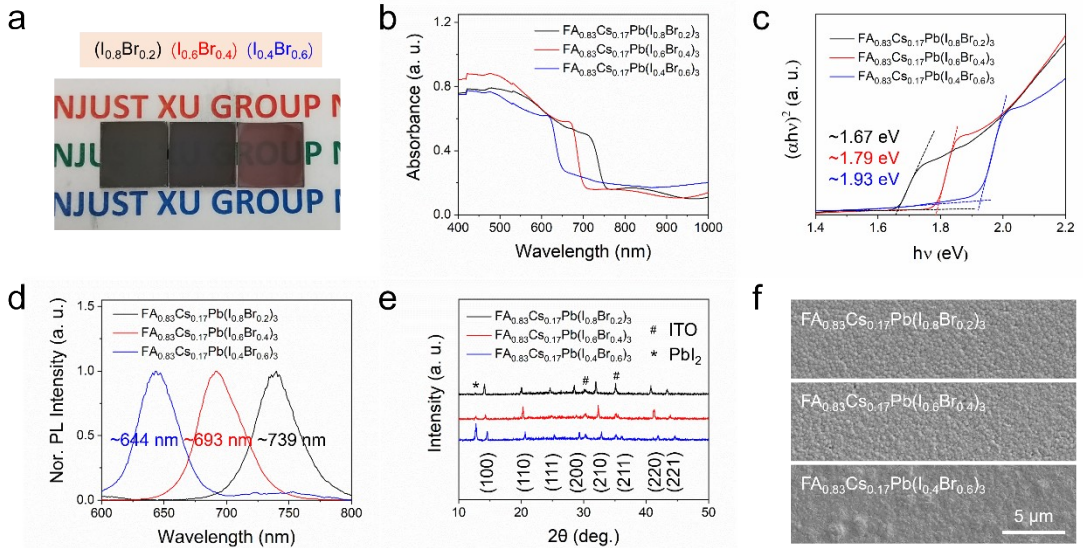


**Fig. S1 Characterizations of  $\text{FA}_{0.83}\text{Cs}_{0.17}\text{Pb}(\text{I}_{1-x}\text{Br}_x)_3$  ( $x = 0.2, 0.4$ , and  $0.6$ ) perovskite films.** (a) Optical photograph. (b) UV-vis absorption spectra, and (c) corresponding Tauc plots. (d) PL spectra. (e) XRD patterns. (f) Top-view SEM images.

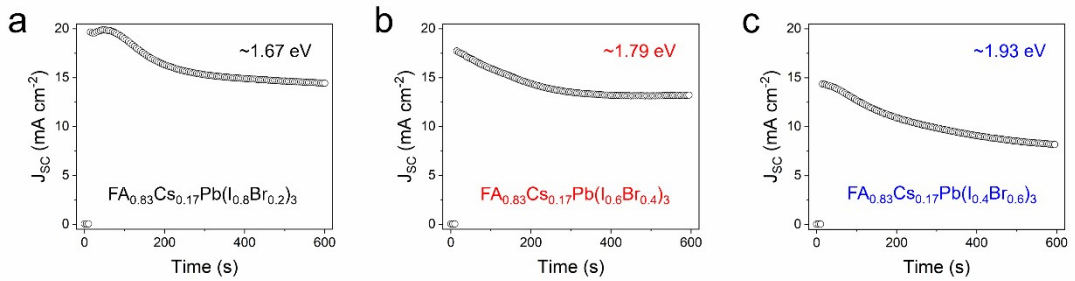


**Fig. S2 Performance degradation of  $\text{FA}_{0.83}\text{Cs}_{0.17}\text{Pb}(\text{I}_{1-x}\text{Br}_x)_3$  ( $x = 0.2, 0.4$  and  $0.6$ ) PSCs under illumination.**

Steady-state  $J_{SC}$  outputs of (a)  $\text{FA}_{0.83}\text{Cs}_{0.17}\text{Pb}(\text{I}_{0.8}\text{Br}_{0.2})_3$ , (b)  $\text{FA}_{0.83}\text{Cs}_{0.17}\text{Pb}(\text{I}_{0.6}\text{Br}_{0.4})_3$ , and (c)  $\text{FA}_{0.83}\text{Cs}_{0.17}\text{Pb}(\text{I}_{0.4}\text{Br}_{0.6})_3$  PSCs, respectively.

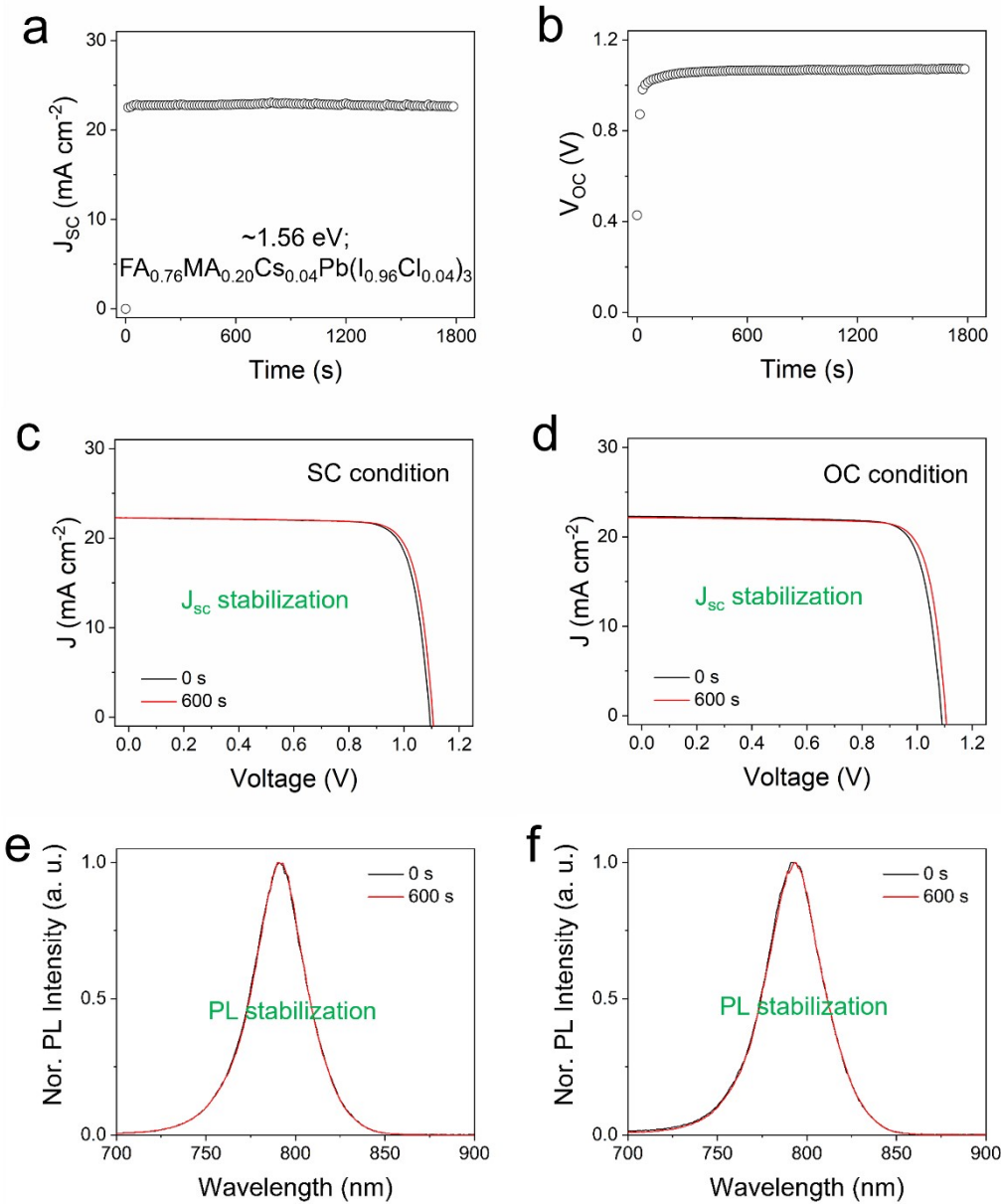


**Fig. S3 Stability evolution of 1.56-eV  $\text{FA}_{0.76}\text{MA}_{0.20}\text{Cs}_{0.04}\text{Pb}(\text{I}_{0.96}\text{Cl}_{0.04})_3$  PSCs under illumination.** (a)  $J_{SC}$  and (b)  $V_{OC}$  outputs of  $\text{FA}_{0.76}\text{MA}_{0.20}\text{Cs}_{0.04}\text{Pb}(\text{I}_{0.96}\text{Cl}_{0.04})_3$  PSCs during 1800 seconds illumination, respectively. J-V curves and corresponding PL spectra before and after 600 seconds illumination under (c, e) SC and (d, f) OC conditions, respectively,

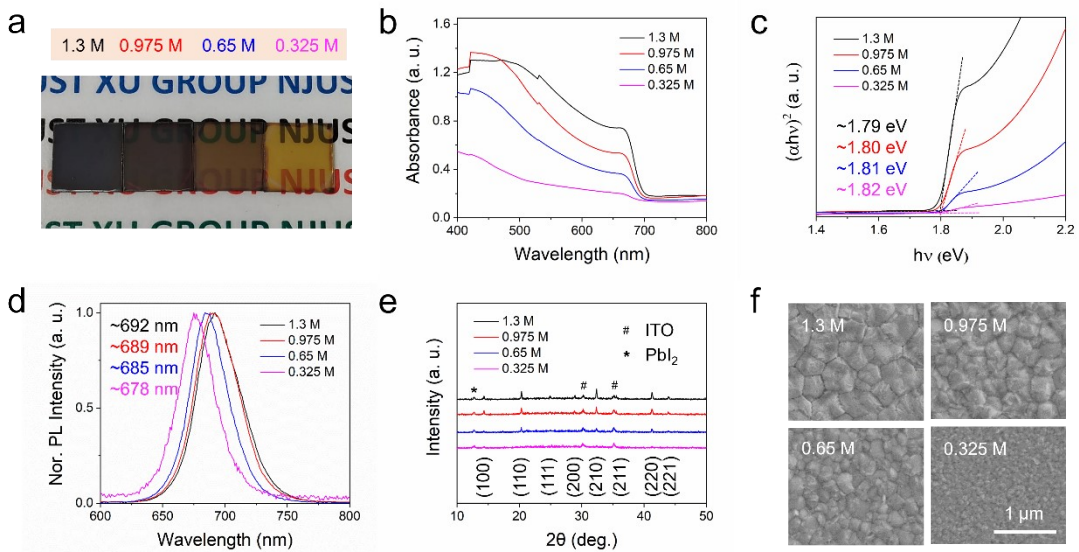


**Fig. S4 Characterizations of  $\text{FA}_{0.83}\text{Cs}_{0.17}\text{Pb}(\text{I}_{0.6}\text{Br}_{0.4})_3$  (precursor concentration: 1.3, 0.975, 0.65, and 0.325 M) perovskite films.** (a) Optical photograph. (b) UV-vis absorption spectra, and (c) corresponding Tauc plots. (d) PL spectra. (e) XRD patterns. (f) Top-view SEM images.

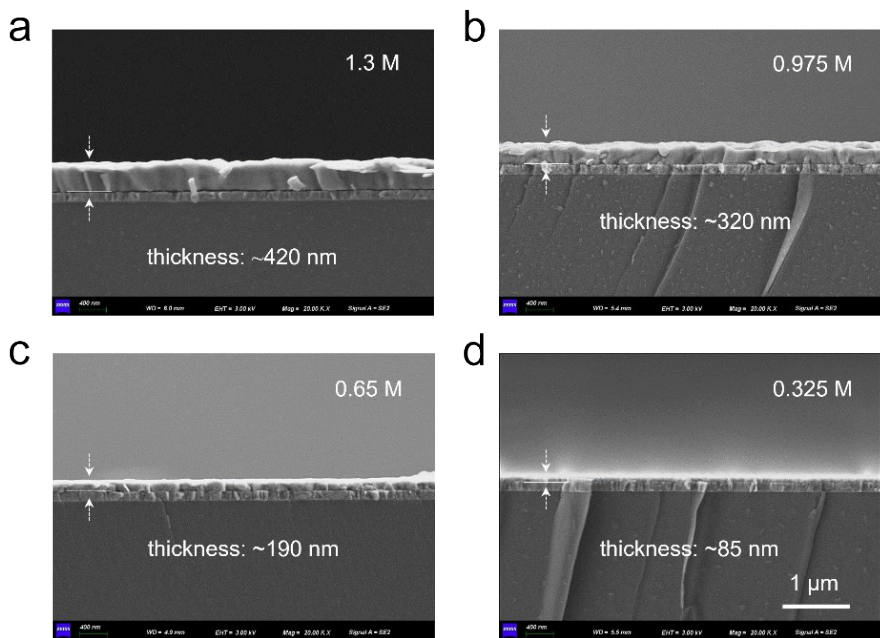


**Fig. S5 Cross-sectional SEM images of  $\text{FA}_{0.83}\text{Cs}_{0.17}\text{Pb}(\text{I}_{0.6}\text{Br}_{0.4})_3$  (precursor concentration: 1.3, 0.975, 0.65, and 0.325 M) perovskite films. The thicknesses of perovskite films are ~420, 320, 190, and 85 nm, respectively.**

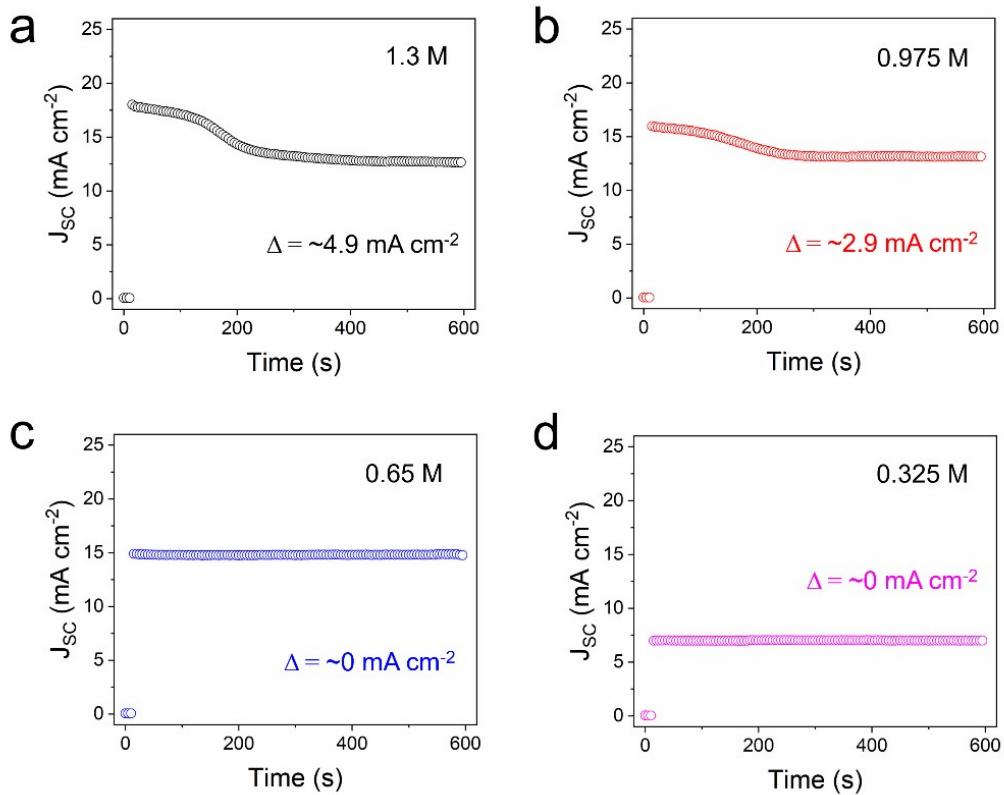


**Fig. S6**  $J_{SC}$  outputs of  $\text{FA}_{0.83}\text{Cs}_{0.17}\text{Pb}(\text{I}_{0.6}\text{Br}_{0.4})_3$  (precursor concentration: **1.3, 0.975, 0.65, and 0.325 M**) PSCs. The  $J_{SC}$  losses of devices are  $\sim 4.9$ ,  $2.9$ ,  $0$ , and  $0 \text{ mA cm}^{-2}$ , respectively.

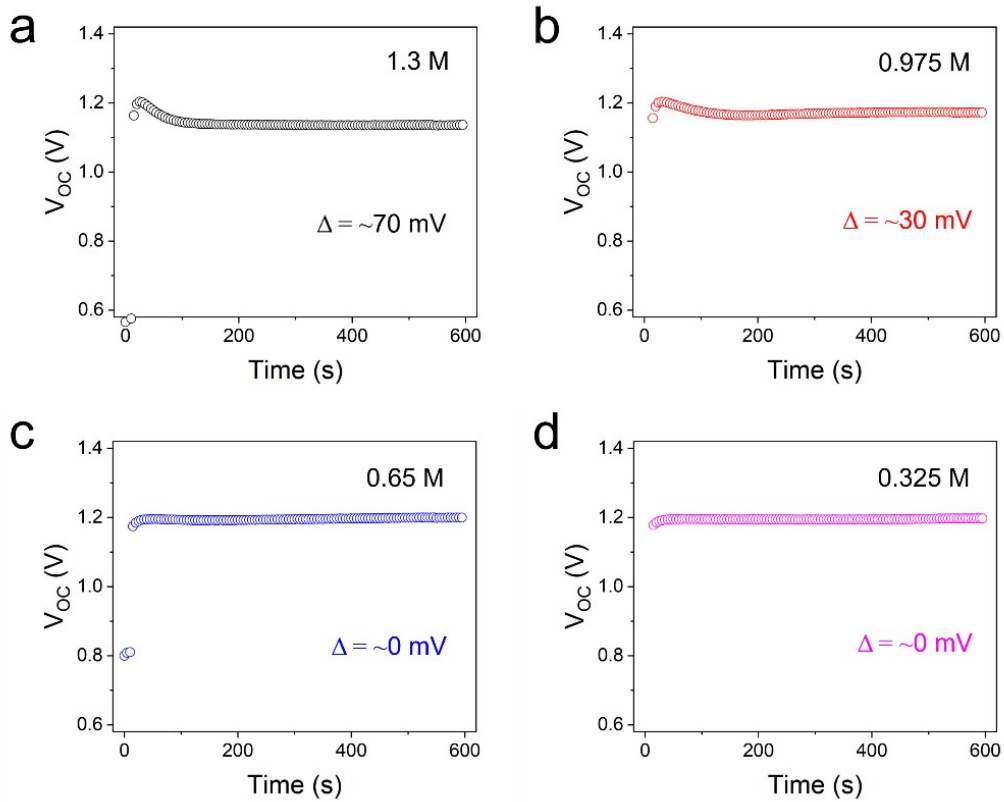


**Fig. S7**  $V_{OC}$  outputs of  $\text{FA}_{0.83}\text{Cs}_{0.17}\text{Pb}(\text{I}_{0.6}\text{Br}_{0.4})_3$  PSCs (precursor concentration: **1.3, 0.975, 0.65, and 0.325 M**). The  $V_{OC}$  deficits of devices are  $\sim 70$ ,  $30$ ,  $0$ , and  $0$  mV, respectively.

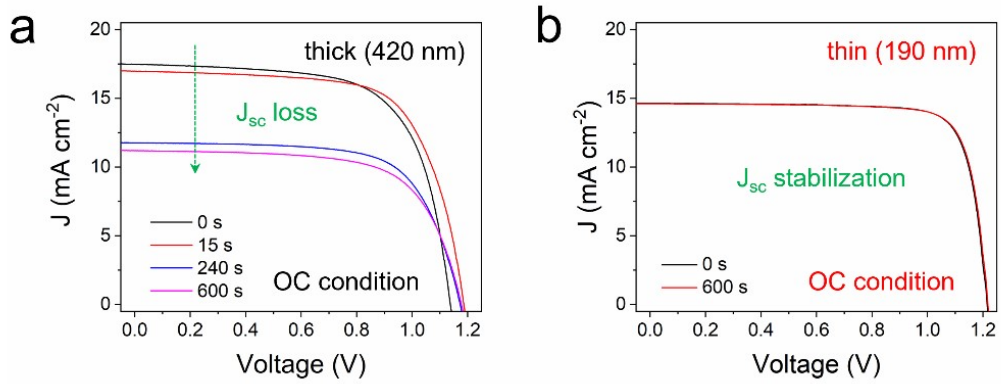


**Fig. S8 Time-dependent J-V curves of  $\text{FA}_{0.83}\text{Cs}_{0.17}\text{Pb}(\text{I}_{0.6}\text{Br}_{0.4})_3$  PSCs with thickness-varying perovskite films under OC condition in Fig. 2.**

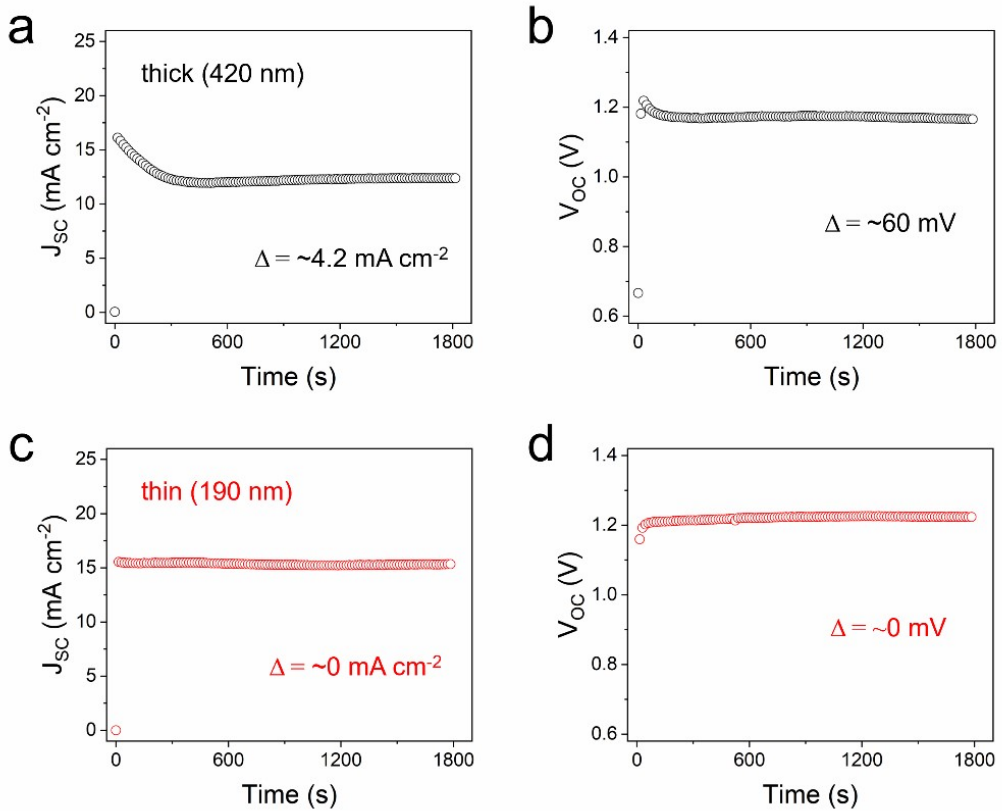


**Fig. S9  $J_{\text{SC}}/V_{\text{OC}}$  outputs of  $\text{FA}_{0.83}\text{Cs}_{0.17}\text{Pb}(\text{I}_{0.6}\text{Br}_{0.4})_3$  PSCs with thickness-varying perovskite films under longer illumination (0 ~ 1800 seconds).** (a, c) The  $J_{\text{SC}}$  losses of devices are  $\sim 4.2$  and  $0 \text{ mA cm}^{-2}$ , respectively. (b, d) The  $V_{\text{OC}}$  deficits of devices are  $\sim 60$  and  $0 \text{ mV}$ , respectively.

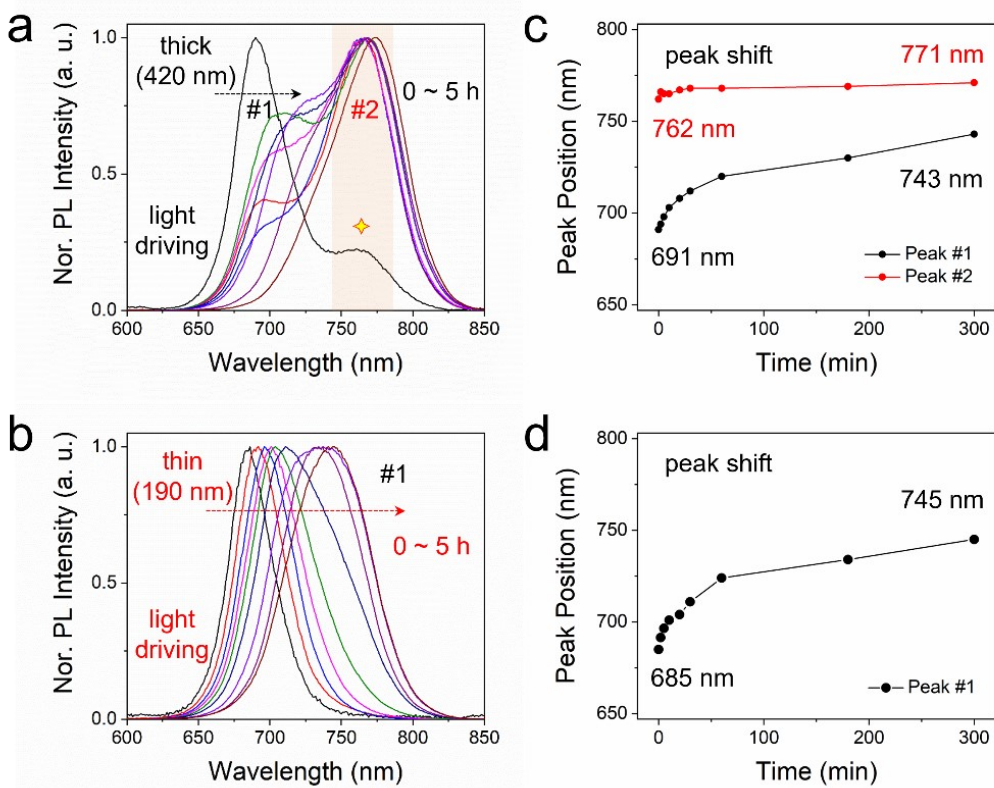


**Fig. S10 Halide segregation phenomenon in thickness-varying  $\text{FA}_{0.83}\text{Cs}_{0.17}\text{Pb}(\text{I}_{0.6}\text{Br}_{0.4})_3$  perovskite films under longer illumination (0 ~ 5 hours).**

(a, b) PL spectra evolution during illumination. (c, d) Corresponding red-shifted trends of PL emission peaks.

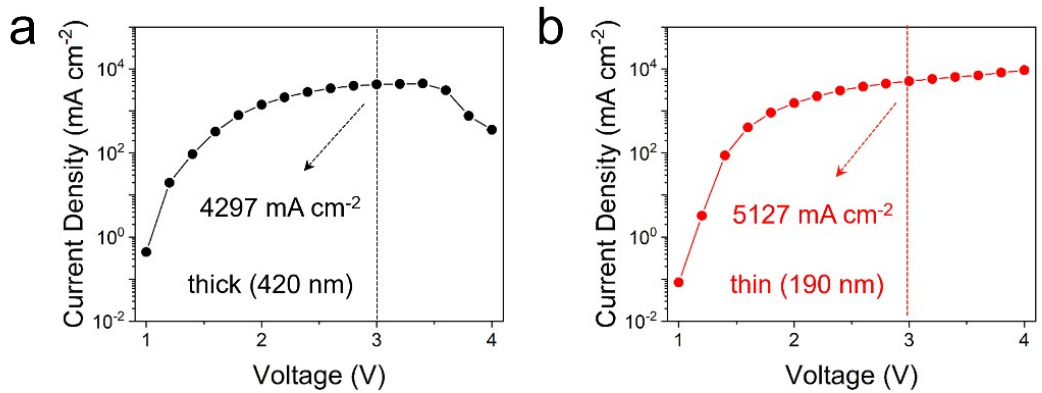


**Fig. S11 Electrical property of  $\text{FA}_{0.83}\text{Cs}_{0.17}\text{Pb}(\text{I}_{0.6}\text{Br}_{0.4})_3$  devices working as LEDs.**

J-V curves of complete devices based on (a) thick and (b) thin perovskite films, respectively, during voltage-driven EL spectra evolution in **Fig. 3**.

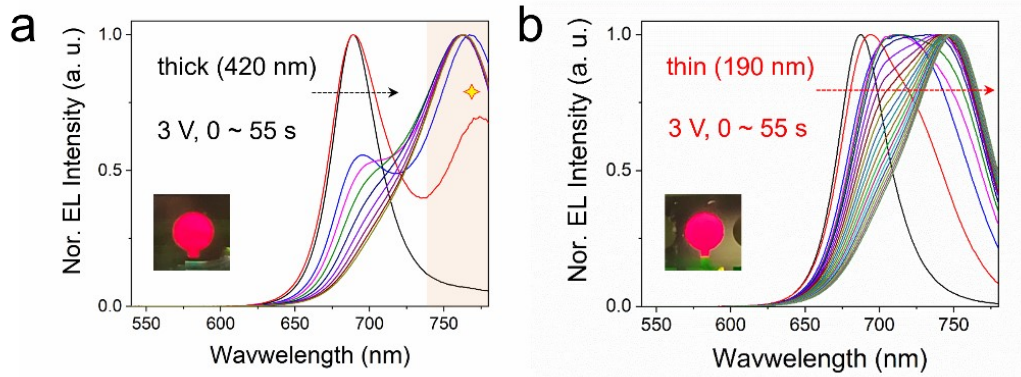


**Fig. S12 Halide segregation phenomenon of  $\text{FA}_{0.83}\text{Cs}_{0.17}\text{Pb}(\text{I}_{0.6}\text{Br}_{0.4})_3$  devices working as LEDs.** EL spectra evolution of complete devices based on (a) thick and (b) thin perovskite films, respectively, at a bias of 3 V.

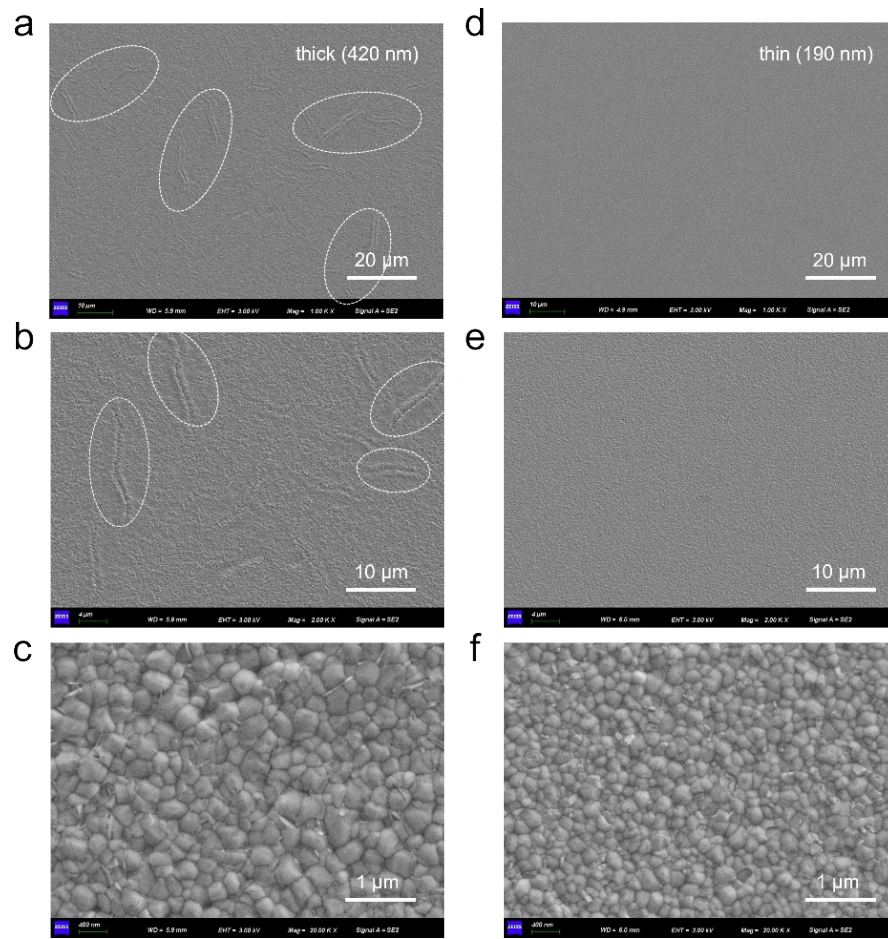


**Fig. S13 Morphology characterization of thickness-varying  $\text{FA}_{0.83}\text{Cs}_{0.17}\text{Pb}(\text{I}_{0.6}\text{Br}_{0.4})_3$  perovskite films.** Top-view SEM images of (a-c) thick and (d-f) thin perovskite films with different magnifications, respectively.

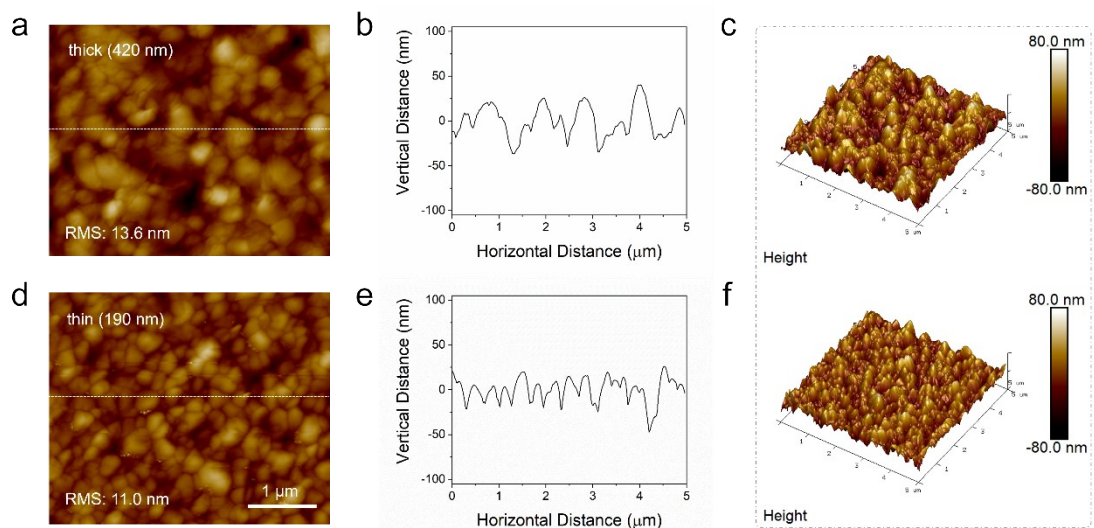


**Fig. S14 Morphology characterization of thickness-varying  $\text{FA}_{0.83}\text{Cs}_{0.17}\text{Pb}(\text{I}_{0.6}\text{Br}_{0.4})_3$  perovskite films.** AFM images of (a-c) thick and (d-f) thin perovskite films, respectively.

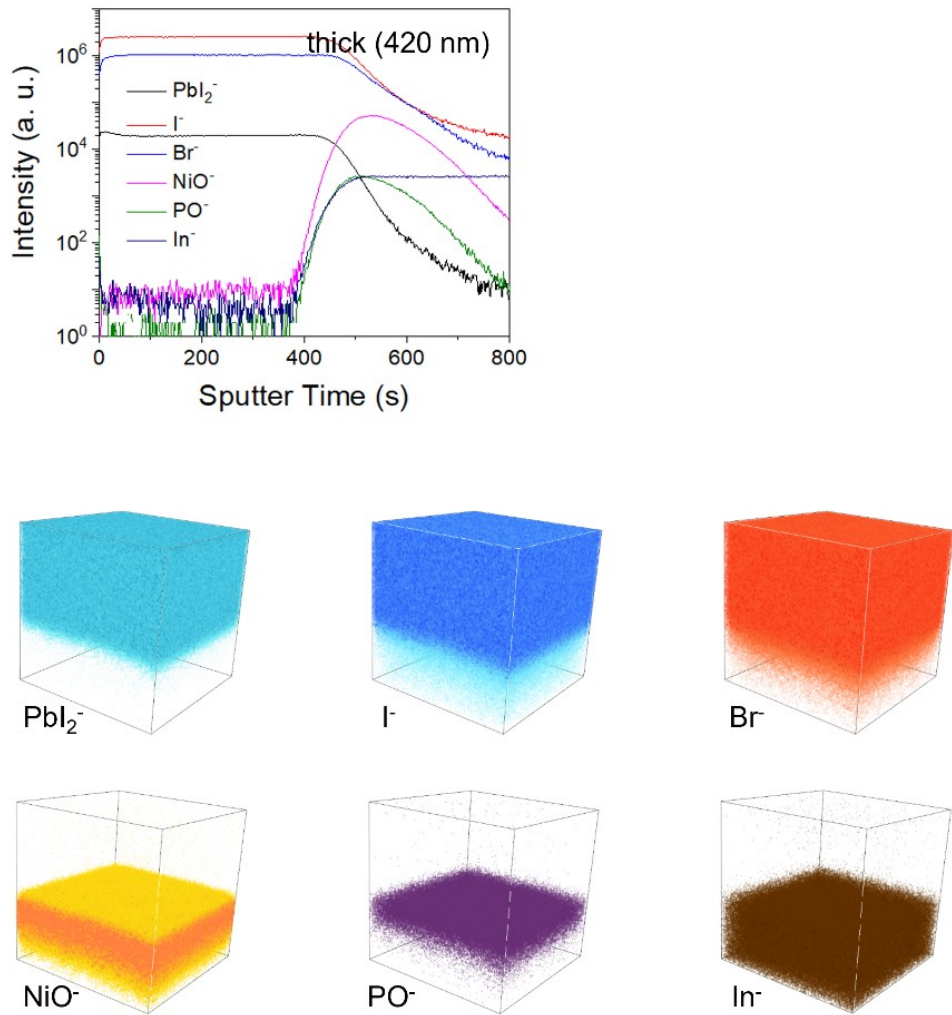


**Fig. S15 Elemental analysis of thick  $\text{FA}_{0.83}\text{Cs}_{0.17}\text{Pb}(\text{I}_{0.6}\text{Br}_{0.4})_3$  perovskite film. TOF-SIMS depth profiles and corresponding mapping images of thick perovskite film.**

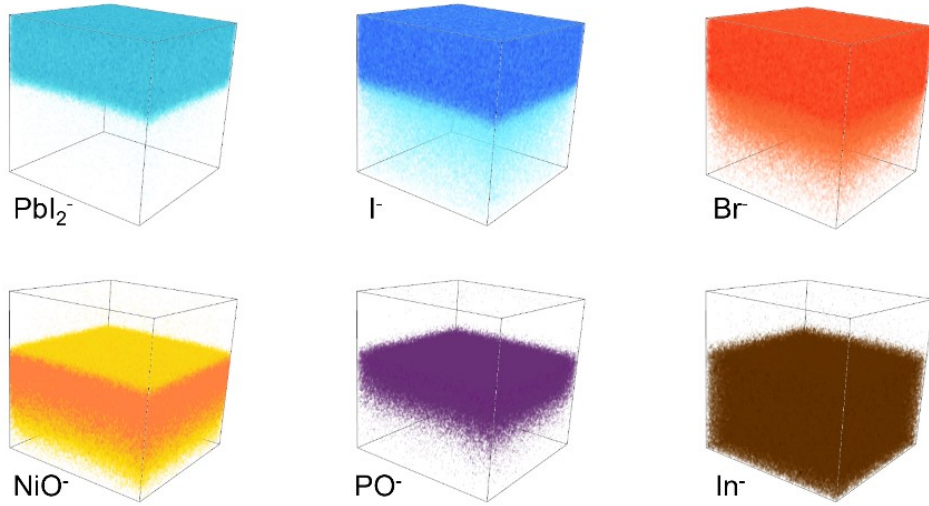
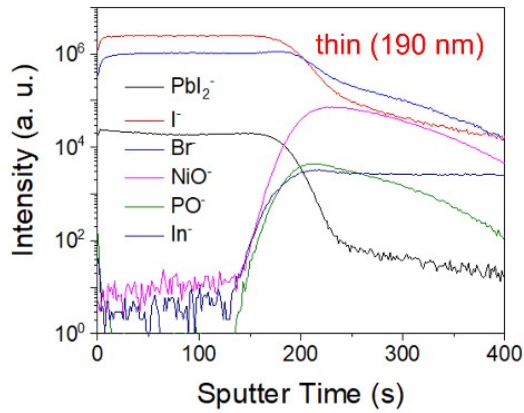


**Fig. S16 Elemental analysis of thin  $\text{FA}_{0.83}\text{Cs}_{0.17}\text{Pb}(\text{I}_{0.6}\text{Br}_{0.4})_3$  perovskite film. TOF-SIMS depth profiles and corresponding mapping images of thin perovskite film.**

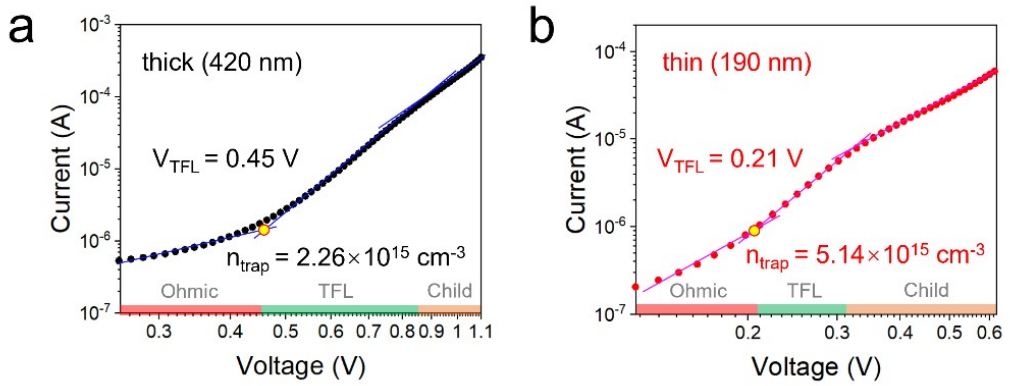


**Fig. S17 Defect calculation for thickness-varying  $\text{FA}_{0.83}\text{Cs}_{0.17}\text{Pb}(\text{I}_{0.6}\text{Br}_{0.4})_3$  perovskite films.** Dark J-V curves of hole-only devices based on (a) thick and (b) thin perovskite films, respectively.

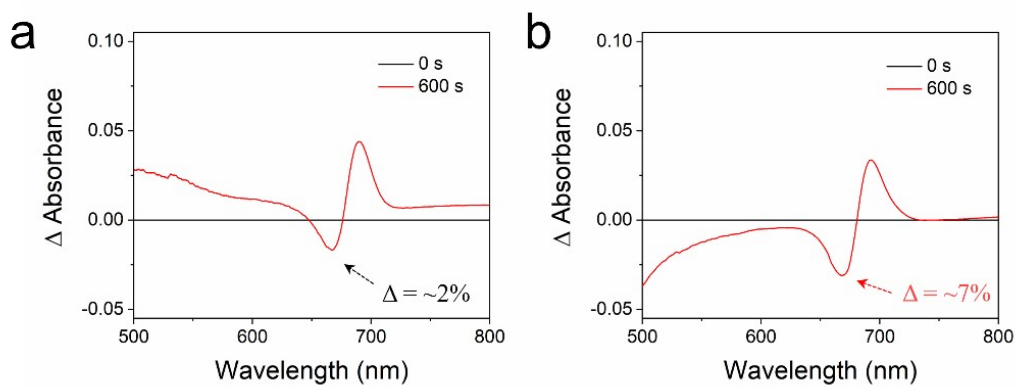


**Fig. S18 Halide segregation of thickness-varying  $\text{FA}_{0.83}\text{Cs}_{0.17}\text{Pb}(\text{I}_{0.6}\text{Br}_{0.4})_3$  perovskite films after light exposure.** Change of UV-vis absorption spectra for (a) thick and (b) thin perovskite films, respectively, after 600 seconds of illumination.

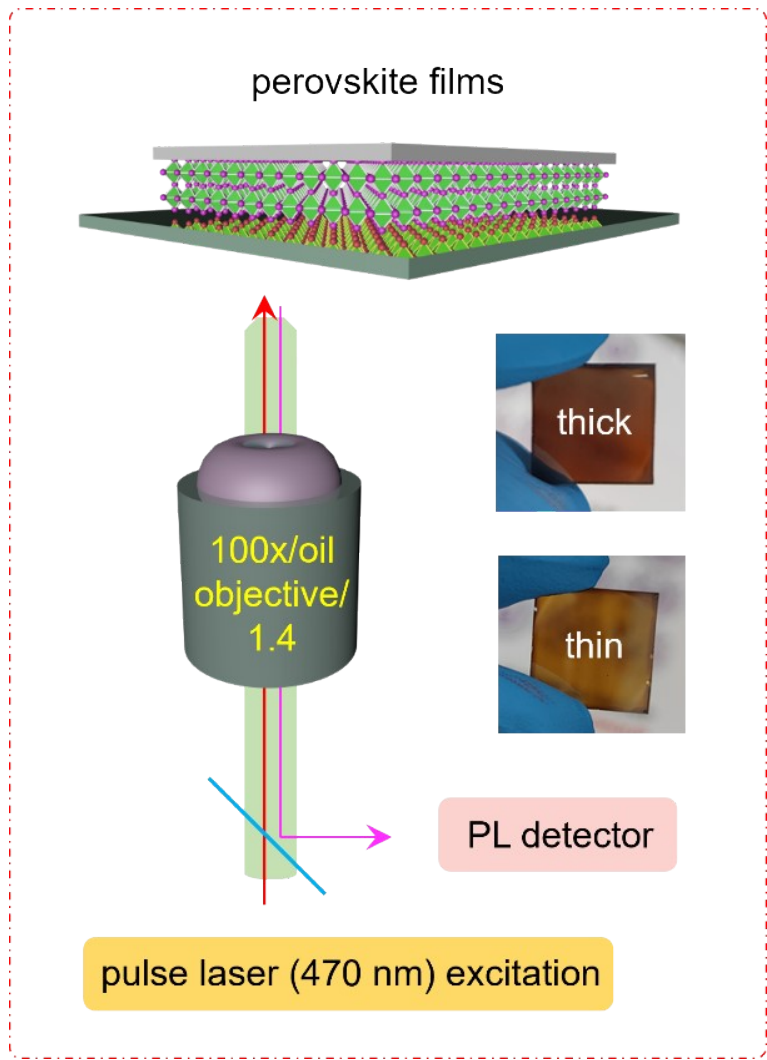


**Fig. S19 Microscopic characterization of  $\text{FA}_{0.83}\text{Cs}_{0.17}\text{Pb}(\text{I}_{0.6}\text{Br}_{0.4})_3$  perovskite films during illumination.** The experiment setup for CLSM measurements and the optical photograph of perovskite films.

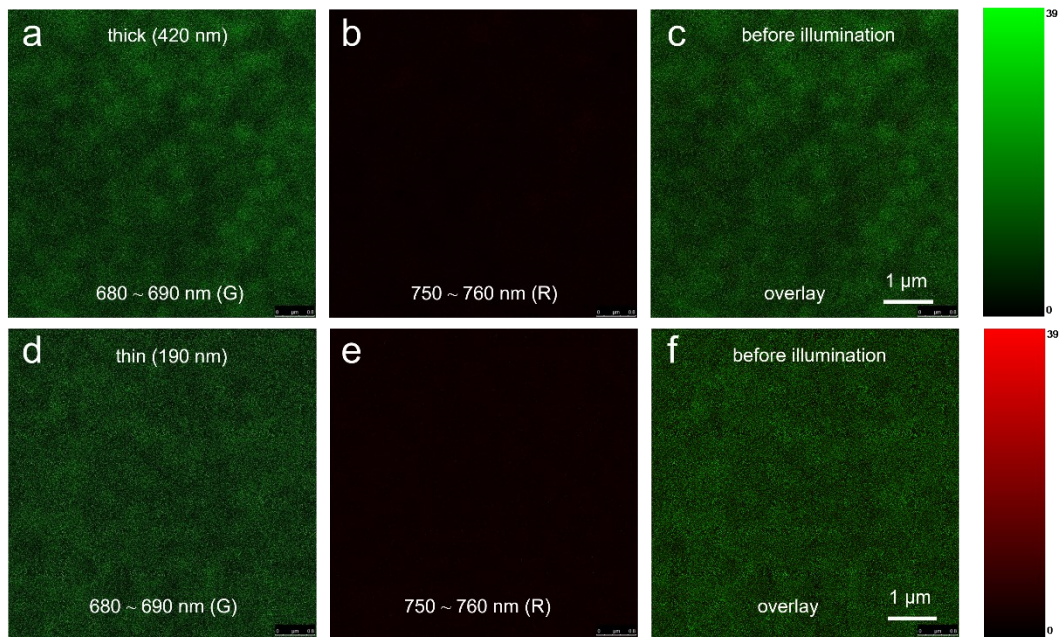


**Fig. S20 Microscopic characterizations of PIHS issue in thickness-varying  $\text{FA}_{0.83}\text{Cs}_{0.17}\text{Pb}(\text{I}_{0.6}\text{Br}_{0.4})_3$  perovskite films.** PL mappings of (a-c) thick and (d-f) thin perovskite films before illumination. Note: the window of 680 ~ 690 nm stands for original or slightly red-shifted phases, and the window of 750 ~ 760 nm stands for I-rich terminal domains.

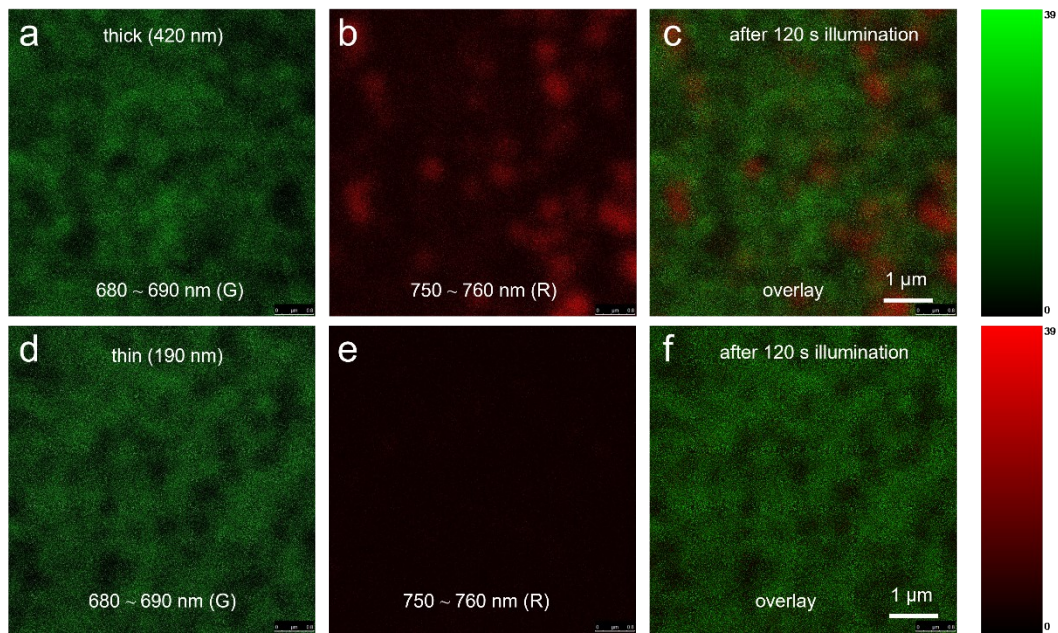


**Fig. S21 Microscopic characterizations of PIHS issue in thickness-varying  $\text{FA}_{0.83}\text{Cs}_{0.17}\text{Pb}(\text{I}_{0.6}\text{Br}_{0.4})_3$  perovskite films.** PL mappings of (a-c) thick and (d-f) thin perovskite films after 120 s illumination. Note: the window of 680 ~ 690 nm stands for original or slightly red-shifted phases, and the window of 750 ~ 760 nm stands for I-rich terminal domains.

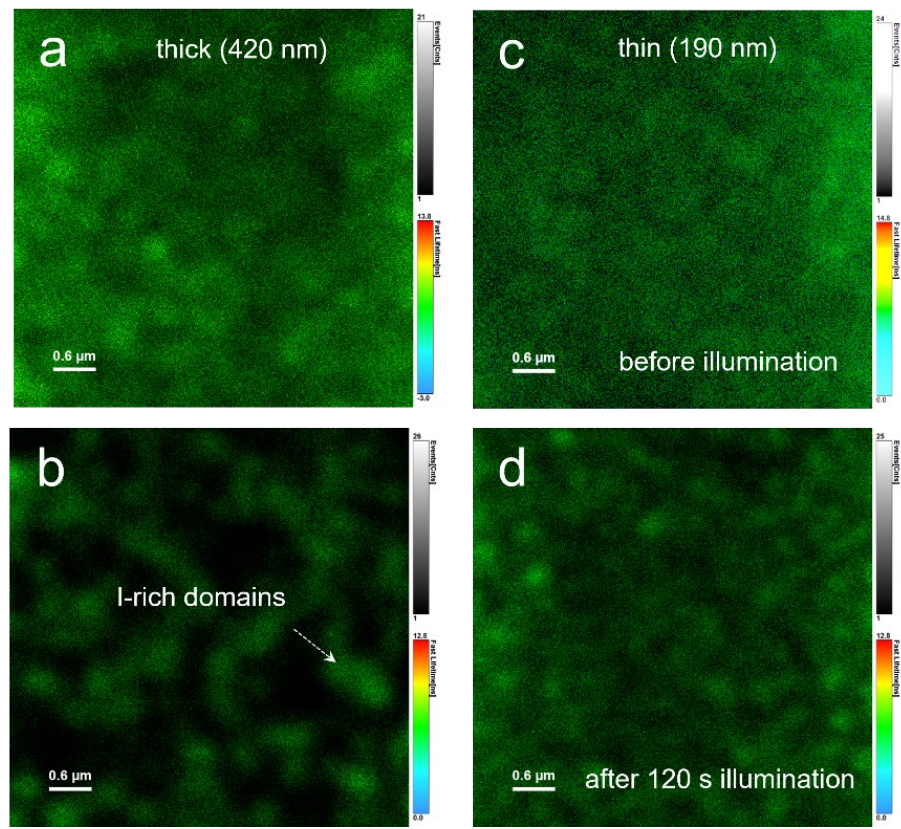


**Fig. S22 Microscopic characterizations of PIHS issue in thickness-varying  $\text{FA}_{0.83}\text{Cs}_{0.17}\text{Pb}(\text{I}_{0.6}\text{Br}_{0.4})_3$  perovskite films.** PL lifetime mapping of (a, b) thick and (c, d) thin perovskite films before and after 120 seconds of illumination.

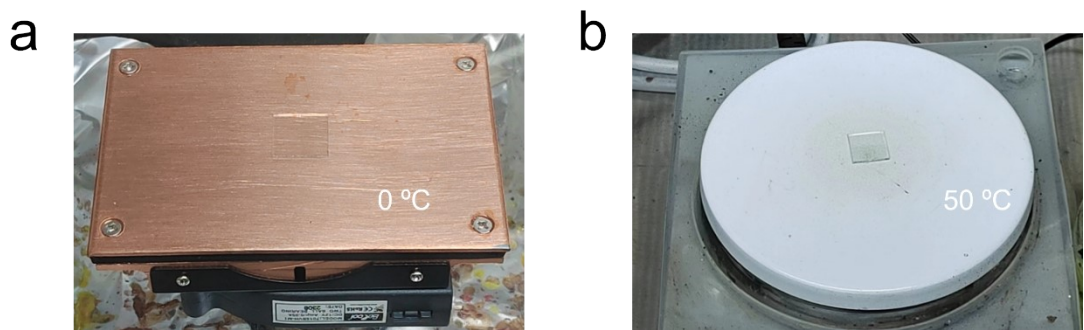


**Fig. S23 Substrate pretreatments before fabrication of  $\text{FA}_{0.83}\text{Cs}_{0.17}\text{Pb}(\text{I}_{0.6}\text{Br}_{0.4})_3$  perovskite films.** (a) 10 minutes precool of 0 °C and 10 minutes preheat of 50 °C.

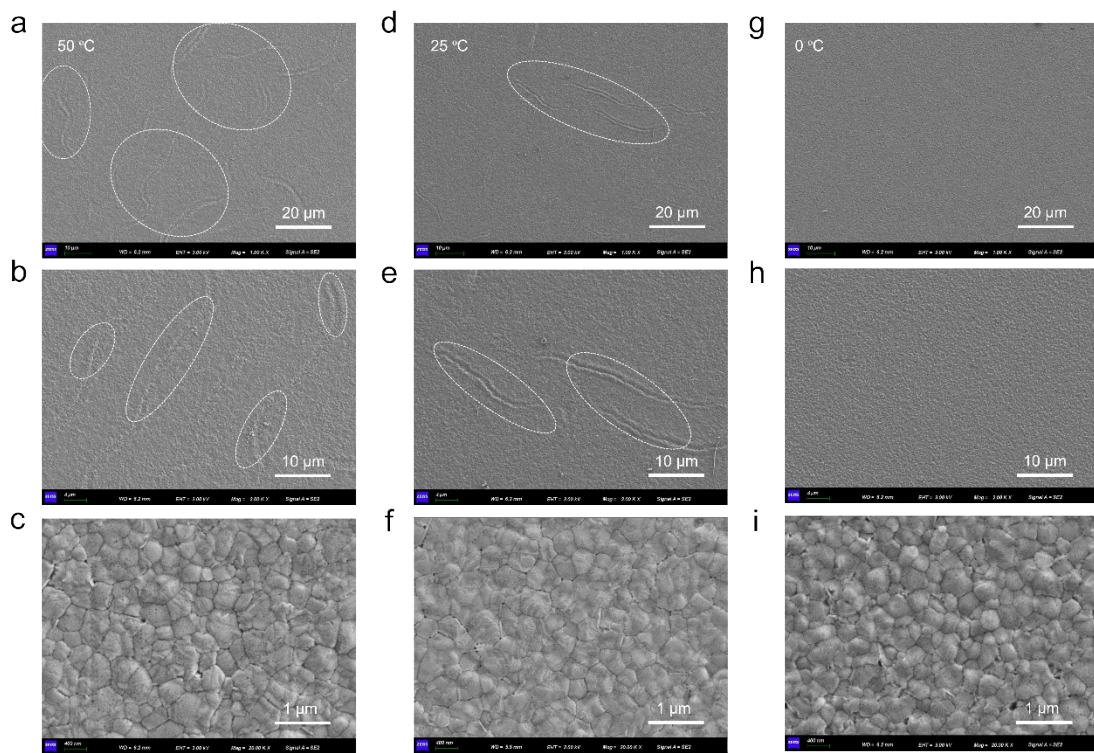


**Fig. S24 Morphology characterization of  $\text{FA}_{0.83}\text{Cs}_{0.17}\text{Pb}(\text{I}_{0.6}\text{Br}_{0.4})_3$  perovskite films with different pretreatments.** Top-view SEM images of perovskite films under conditions of (a-c) 50, (d-f) 25, and (g-i) 0 °C, respectively.

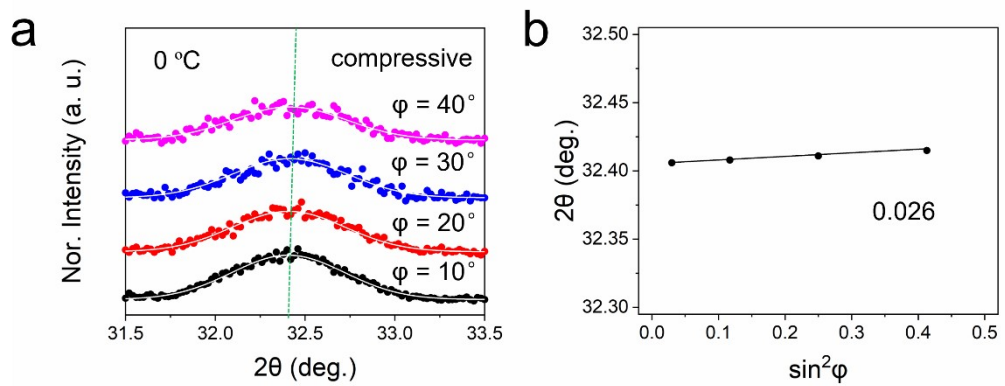


**Fig. S25 Strain analysis of  $\text{FA}_{0.83}\text{Cs}_{0.17}\text{Pb}(\text{I}_{0.6}\text{Br}_{0.4})_3$  perovskite films fabricated under 10-min precool of 0 °C.** (a) GIXRD patterns with an incident angle of 1° at different  $\varphi$  angles ( $10 \sim 40^\circ$ ) and Gauss fitted lines (white). (b) Shift in peak positions plotted against  $\varphi$  angle.

**Table S1.** Summary of the related literatures on exploring the relationship between performance degradation (i.e. J/V loss) of WBG PSCs and PIHS issue, as well as some representative work based on Br-free perovskites for comparison.

In detail, this summary aims at reviewing the research process and mechanisms about PIHS-induced  $V_{OC}$  and  $J_{SC}$  losses, as well as proposing the potential challenges about this issue, which may help present the novelty and interpretations of our work after comparison.

**For  $V_{OC}$  deficit:** By 2015, the reasons for voltage deficit ( $>500$  mV) are unclear in Br-rich WBG PSCs. Until the discovery of PIHS issue from Hoke et al., this appearance has been always applied to account for  $V_{OC}$  deficits, but the related mechanism and precise extent of this influence remain undefined. In 2020, the work from Snaith's group combined Fourier transform photocurrent spectroscopy with detailed balance calculations to first quantify the voltage loss from PIHS issue. However, results indicate that PIHS issue is not the dominant  $V_{OC}$  loss mechanism. Rather, the loss is dominated by the low radiative efficiency, caused by imperfections within the absorber layer and at the perovskite/CTMs heterojunctions. Based on this viewpoint, more experiment and theory are necessary to clarify the relationship between  $V_{OC}$  deficit and PIHS issue.

**For  $J_{SC}$  loss:** Over the past few years, researchers discover that there is also a terrible photostability of  $J_{SC}$  output, apart from voltage deficit, ultimately deteriorating device efficiency. In 2021, Janssen's group put forward that the devices instead deteriorate by a  $J_{SC}$  loss and the  $V_{OC}$  output is less affected. Localization of photogenerated charge carriers in I-rich domains and subsequent recombination cause reduced photocurrent. Meanwhile, the work from Li's group supposed that I-rich phases primarily segregated at defect-enriched grain boundaries could result in  $J_{SC}$  loss under

continuous illumination. However, the specific mechanism between these two factors is waiting for more experimental evidence.

**Advances of our work: Initial  $J_{SC}$  Loss and Efficiency Decline:** In contrast to the relatively minor  $V_{OC}$  deficit (<100 mV; direct evidence to the standpoint from Snaith's group), a sharp loss in  $J_{SC}$  during the initial stage (~240 seconds) plays a more significant role in the observed decline in PCE. **Dual Halide Migration Modes:** We reveal two distinct migration modes of halide ions: 1) rapid formation of I-rich terminal domains (~760 nm; ~1.63 eV) in thick/crystal-stacked perovskite films; 2) gradually red-shifted I-rich phases in thin/crystal-vertically-oriented perovskite films.

**Mechanisms about PIHS-induced J/V Loss:** The rapid formation of I-rich terminal domains seriously worsens the device  $J_{SC}$  and PCE outputs, but not the gradually red-shifted I-rich phases.

Compared to the indefinite conclusions from previous reports, our findings provide more reliable experimental evidences and a deeper insight into the impact of PIHS on device degradation, offering practical approaches for achieving output-stable WBG PSCs.

PV performance	Year	Timescale for J/V loss	Relationship between J/V loss and PIHS issue	Perovskite component	$E_g$ (eV)	Film property (technology/thickness)	Cell structure	Testing condition	Ref.
$V_{OC}$ deficit	2016	~130 mV loss in 150 s	Unclear	MAPbI <sub>1.3</sub> Br <sub>1.7</sub>	1.90	Two-step process	p-i-n	$V_{OC}$ decay/ AM 1.5	<sup>2</sup>
	2017	>100 mV loss in 36 h	Unclear	MAPbI <sub>2</sub> Br	1.73	Spin-coating	n-i-p	J-V curve/ AM 1.5	<sup>3</sup>
	2018	14/23 mV loss in 10 min	Unclear	Cs <sub>x</sub> FA <sub>1-x</sub> Pb(Br <sub>y</sub> I <sub>1-y</sub> ) <sub>3</sub>	1.68\1.75	Spin-coating	p-i-n	$V_{OC}$ decay/ AM 1.5	<sup>4</sup>
	2018	~200 mV loss in 180 s	Unclear	MAPb(I <sub>0.6</sub> Br <sub>0.4</sub> ) <sub>3</sub>	1.80	Spin-coating	p-i-n	$V_{OC}$ decay/ AM 1.5	<sup>5</sup>
	2021	~100 mV loss in 600 s	Unclear	CsPbBr <sub>1.5</sub> I <sub>1.5</sub>	2.04	Spin-coating	n-i-p	$V_{OC}$ decay/ AM 1.5	<sup>6</sup>
	2020	~75 mV loss in 120 min	The $V_{OC}$ loss mainly results from low radiative efficiency, but not halide segregation.	FA <sub>0.83</sub> MA <sub>0.17</sub> Pb(I <sub>0.4</sub> Br <sub>0.6</sub> ) <sub>3</sub>	1.77	Spin-coating	n-i-p	$V_{OC}$ decay/ AM 1.5	<sup>7</sup>
	2020	---	The I-rich domains is not the primary reason for $V_{OC}$ loss; rather, it is caused by a high interfacial defect density and partial energy alignment issues.	Cs <sub>0.05</sub> (FA <sub>x</sub> MA <sub>y</sub> ) <sub>0.95</sub> Pb(I <sub>x</sub> Br <sub>y</sub> ) <sub>3</sub>	1.52-1.88	Spin-coating	p-i-n	J-V curve/ AM 1.5	<sup>8</sup>
	2022	---	Unclear	Cs <sub>0.17</sub> FA <sub>0.83</sub> PbI <sub>3-x</sub> Br <sub>x</sub>	1.65-1.86	Spin-coating/~500 nm	p-i-n	J-V curve/ LED 3000 K 1000 lux	<sup>9</sup>
	2023	---	Unclear	Cs <sub>0.05</sub> (FA <sub>0.6</sub> MA <sub>0.4</sub> ) <sub>0.95</sub> Pb(I <sub>0.6</sub> Br <sub>0.4</sub> ) <sub>3</sub>	1.80	Spin-coating	p-i-n	J-V curve/ AM 1.5G	<sup>10</sup>

$J_{SC}$ loss	2016	$\sim 4 \text{ mA cm}^{-2}$ loss in 150 s	Unclear	MAPbI <sub>1.3</sub> Br <sub>1.7</sub>	1.90	Two-step process	p-i-n	$J_{SC}$ decay/AM 1.5	<sup>2</sup>
	2020	50% drop in 4000 s	Unclear	Cs <sub>0.2</sub> FA <sub>0.8</sub> PbI <sub>0.9</sub> Br <sub>2.1</sub>	1.99	Spin-coating/~180 nm	p-i-n	MPPt tracking/AM 1.5G	<sup>11</sup>
	2021	$\sim 12.5 \text{ mA cm}^{-2}$ loss in 28 h	The cells instead deteriorate by a loss of $J_{SC}$ and that the $V_{OC}$ is less affected.	FA <sub>0.66</sub> MA <sub>0.34</sub> Pb(I <sub>0.67</sub> Br <sub>0.33</sub> ) <sub>3</sub>	1.75	Two-step process	p-i-n	J-V curve/100 mW cm <sup>-2</sup> of visible light	<sup>12</sup>
	2023	$\sim 2 \text{ mA cm}^{-2}$ loss in 8 s	Without	FA <sub>85</sub> Cs <sub>15</sub> Pb(I <sub>60</sub> Br <sub>40</sub> ) <sub>3</sub>	1.80	Spin-coating	p-i-n	$J_{SC}$ decay/AM 1.5G	<sup>13</sup>
	2023	$\sim 3.5 \text{ mA cm}^{-2}$ loss in 40 h	Unclear	Cs <sub>0.2</sub> FA <sub>0.8</sub> Pb(I <sub>0.6</sub> Br <sub>0.4</sub> ) <sub>3</sub>	1.78	Spin-coating/~350 nm	p-i-n	J-V curve/AM 1.5G	<sup>14</sup>
	2023	$\sim 2 \text{ mA cm}^{-2}$ loss in 150 min	Unclear	Cs <sub>0.1</sub> FA <sub>0.9</sub> PbBr <sub>2.1</sub> I <sub>0.9</sub>	2.00	Spin coating/~550 nm	p-i-n	J-V curve/AM 1.5G	<sup>15</sup>
	2023	20% drop in 60 min	Unclear	CsPbI <sub>1.4</sub> Br <sub>1.6</sub>	2.00	Spin coating/~280 nm	p-i-n	MPPt tracking/AM 1.5G	<sup>16</sup>
	2024	$\sim 6 \text{ mA cm}^{-2}$ loss in 90 min	Unclear	Cs <sub>0.17</sub> FA <sub>0.83</sub> Pb(I <sub>0.8</sub> Br <sub>0.2</sub> ) <sub>3</sub>	1.67	Spin coating/~480 nm	p-i-n	J-V curve/AM 1.5G	<sup>17</sup>
	2024	$\sim 7 \text{ mA cm}^{-2}$ loss in 90 min	Without	Cs <sub>0.05</sub> (FA <sub>0.83</sub> MA <sub>0.17</sub> ) <sub>0.9</sub> <sub>5</sub> Pb(I <sub>0.83</sub> Br <sub>0.17</sub> ) <sub>3</sub>	1.63	Spin-coating	n-i-p	J-V curve/AM 1.5G	<sup>18</sup>
	$\sim 6 \text{ mA cm}^{-2}$ loss in 600 s		1. In contrast to the relatively minor $V_{OC}$ deficit (<100 mV), a sharp loss in $J_{SC}$ during the initial stage (~240 seconds) plays a more significant role in the observed decline in PCE.	Cs <sub>0.17</sub> FA <sub>0.83</sub> Pb(I <sub>0.8</sub> Br <sub>0.2</sub> ) <sub>3</sub>	1.67	Spin coating			
$\sim 5.8 \text{ mA cm}^{-2}$ loss in 600 s		2. There are two distinct	Cs <sub>0.17</sub> FA <sub>0.83</sub> Pb(I <sub>0.6</sub> Br <sub>0.4</sub> ) <sub>3</sub>	1.79	Spin coating/~420 nm				
Without loss in 600 s						Spin coating/~190 nm			

migration modes of rapid formation of I-rich terminal domains ( $\sim 760$  nm;  $\sim 1.63$  eV) and gradually red-shifted I-rich phases.

3. The rapid formation of I-rich terminal domains seriously affects the device  $J_{SC}$  and PCE outputs, but not the gradually red-shifted I-rich phases.

							J-V curve/ AM 1.5G	19
Stable J/V output	2018	Without loss in $>150$ min	Without	$FA_{0.7}MA_{0.25}Cs_{0.05}PbI_3$	1.56	Hot casting	p-i-n	MPPt tracking/ AM 1.5G
	2023	Almost no loss in 600 s	Without	$Cs_{0.06}MA_{0.14}FA_{0.80}PbI_3$	1.55	Spin coating	p-i-n	MPPt tracking/ AM 1.5G
	2024	5.8% drop in 1000 h	Without	$Cs_{0.05}(FA_{0.98}MA_{0.02})_{0.9}PbI_3$	1.55	Spin coating	p-i-n	MPPt tracking/ AM 1.5G

**Table S2.** Material's bandgap used in tandem and triple-junction devices from the literatures (this table is the source for data points shown in Fig. 1a).

Device structure	E <sub>g</sub> -top (eV)	E <sub>g</sub> -middle (eV)	E <sub>g</sub> -bottom (eV)	Ref.	Record PCE (%)
Perovskite		1.55		21	
		1.56		22	26.7
Perovskite/Si	1.63		1.10	23	
	1.67		1.10	24	
	1.66		1.10	25	
	1.68		1.10	26	
	1.63		1.10	27	
	1.68		1.10	28	
	1.63		1.10	29	34.2
	1.68		1.10	30	
	1.63		1.10	31	
	1.63		1.10	32	
Perovskite/Perovskite	1.65		1.10	33	
	1.62		1.10	34	
	1.79		1.25	35	
	1.79		1.24	36	
	1.71		1.27	37	
	1.77		1.26	38	
	1.80		1.22	39	
	1.73		1.22	40	
	1.77		1.25	41	
	1.80		1.26	42	30.1
Perovskite/Organic	1.78		1.25	43	
	1.77		1.22	44	
	1.77		1.22	45	
	1.78		1.25	46	
	1.77		1.22	47	
	1.81		1.33	48	25.06

	1.78	1.22	<sup>49</sup>		
	1.98	1.32	<sup>50</sup>		
	1.92	1.47	<sup>51</sup>		
	1.79	1.36	<sup>52</sup>		
	1.85	1.33	<sup>53</sup>		
	1.79	1.3	<sup>54</sup>		
	1.84	1.38	<sup>55</sup>		
<hr/>					
	1.68	1.10	<sup>56</sup>		
	1.61	1.02	<sup>57</sup>		
	1.66	1.10	<sup>58</sup>		
	1.68	1.10	<sup>59</sup>		
Perovskite/CIGS	1.68	1.10	<sup>60</sup>	24.2	
	1.58	1.02	<sup>61</sup>		
	1.68	1.12	<sup>62</sup>		
	1.60	1.10	<sup>63</sup>		
	1.59	1.00	<sup>64</sup>		
<hr/>					
	1.96	1.53	1.12	<sup>65</sup>	
	2.00	1.52	1.10	<sup>15</sup>	
Perovskite/Perovskite	1.96	1.56	1.10	<sup>66</sup>	
/Si	1.90	1.55	1.10	<sup>67</sup>	27.1
	1.77	1.55	1.12	<sup>68</sup>	
	1.84	1.52	1.10	<sup>69</sup>	
	1.93	1.55	1.10	<sup>70</sup>	
<hr/>					
	2.00	1.62	1.22	<sup>16</sup>	
Perovskite/Perovskite	1.97	1.61	1.25	<sup>71</sup>	
/Perovskite	1.99	1.60	1.22	<sup>11</sup>	23.8
	1.73	1.57	1.23	<sup>72</sup>	
	1.94	1.57	1.34	<sup>73</sup>	
<hr/>					
Perovskite/Perovskite	2.05	1.62	1.33	<sup>74</sup>	19.4
/Organic					

## Note S1

The trap state densities ( $n_{\text{trap}}$ ) of hole-only devices with a structure of ITO/NiO<sub>x</sub>/2PACz/FA<sub>0.83</sub>Cs<sub>0.17</sub>Pb(I<sub>0.6</sub>Br<sub>0.4</sub>)<sub>3</sub>/PEAI/MoO<sub>x</sub>/Ag were quantified from SCLC testing. The  $n_{\text{trap}}$  values can be determined by trap-filled limit voltage ( $V_{\text{TFL}}$ ) as the following equation:

$$n_{\text{trap}} = \frac{2\epsilon\epsilon_0 V_{\text{TFL}}}{ed^2} \quad (1)$$

where  $\epsilon$  is the relative dielectric constant,<sup>75</sup>  $\epsilon_0$  is the constant of the vacuum permittivity in free space, d is the film thickness, and e is an electron charge. The  $V_{\text{TFL}}$  values are determined to be ~0.45 and 0.21 V from the intersection points, respectively. Subsequently, the target  $n_{\text{trap}}$  values are calculated to be ~2.26 and  $5.14 \times 10^{15}$  cm<sup>-3</sup>, respectively.

## References

- 1 Y. Guo, S. Guo, T. Wu, S. Zhan, C. Wei, X. Luo, J. Huang, J. Su, Y. Hua and B. Xu, *Chem. Eng. J.*, 2024, **497**, 154722.
- 2 X. Yang, X. Yan, W. Wang, X. Zhu, H. Li, W. Ma and C. Sheng, *Org. Electron.*, 2016, **34**, 79-83.
- 3 T. Duong, H. K. Malmudi, Y. Wu, X. Fu, H. Shen, J. Peng, N. Wu, H. T. Nguyen, D. Macdonald, M. Lockrey, T. P. White, K. Weber and K. Catchpole, *ACS Appl. Mater. Interfaces*, 2017, **9**, 26859-26866.
- 4 K. A. Bush, K. Frohma, R. Prasanna, R. E. Beal, T. Leijtens, S. A. Swifter and M. D. McGehee, *ACS Energy Lett.*, 2018, **3**, 428-435.
- 5 A. Rajagopal, R. J. Stoddard, S. B. Jo, H. W. Hillhouse and A. K. Jen, *Nano Lett.*, 2018, **18**, 3985-3993.
- 6 L. Hu, X. Guan, W. Chen, Y. Yao, T. Wan, C.-H. Lin, N. D. Pham, L. Yuan, X. Geng, F. Wang, C.-Y. Huang, J. Yuan, S. Cheong, R. D. Tilley, X. Wen, D. Chu, S. Huang and T. Wu, *ACS Energy Lett.*, 2021, **6**, 1649-1658.
- 7 S. Mahesh, J. M. Ball, R. D. J. Oliver, D. P. McMeekin, P. K. Nayak, M. B. Johnston and H. J. Snaith, *Energy Environ. Sci.*, 2020, **13**, 258-267.
- 8 F. Peña-Camargo, P. Caprioglio, F. Zu, E. Gutierrez-Partida, C. M. Wolff, K. Brinkmann, S. Albrecht, T. Riedl, N. Koch, D. Neher and M. Stolterfoht, *ACS Energy Lett.*, 2020, **5**, 2728-2736.
- 9 C. Zhang, C. Liu, Y. Gao, S. Zhu, F. Chen, B. Huang, Y. Xie, Y. Liu, M. Ma, Z. Wang, S. Wu, R. E. I. Schropp and Y. Mai, *Adv. Sci.*, 2022, **9**, 2204138.
- 10 J. Thiesbrummel, F. Peña-Camargo, K. O. Brinkmann, E. Gutierrez-Partida, F. Yang, J. Warby, S. Albrecht, D. Neher, T. Riedl, H. J. Snaith, M. Stolterfoht and F. Lang, *Adv. Energy Mater.*, 2023, **13**, 2202674.

- 11 K. Xiao, J. Wen, Q. Han, R. Lin, Y. Gao, S. Gu, Y. Zang, Y. Nie, J. Zhu, J. Xu and H. Tan, *ACS Energy Lett.*, 2020, **5**, 2819-2826.
- 12 K. Datta, B. T. van Gorkom, Z. Chen, M. J. Dyson, T. P. A. van der Pol, S. C. J. Meskers, S. Tao, P. A. Bobbert, M. M. Wienk and R. A. J. Janssen, *ACS Appl. Energy Mater.*, 2021, **4**, 6650-6658.
- 13 P. Caprioglio, J. A. Smith, R. D. J. Oliver, A. Dasgupta, S. Choudhary, M. D. Farrar, A. J. Ramadan, Y. H. Lin, M. G. Christoforo, J. M. Ball, J. Diekmann, J. Thiesbrummel, K. A. Zaininger, X. Shen, M. B. Johnston, D. Neher, M. Stolterfoht and H. J. Snaith, *Nat. Commun.*, 2023, **14**, 932.
- 14 J. Wen, Y. Zhao, P. Wu, Y. Liu, X. Zheng, R. Lin, S. Wan, K. Li, H. Luo, Y. Tian, L. Li and H. Tan, *Nat. Commun.*, 2023, **14**, 7118.
- 15 F. Xu, E. Aydin, J. Liu, E. Ugur, G. T. Harrison, L. Xu, B. Vishal, B. K. Yildirim, M. Wang, R. Ali, A. S. Subbiah, A. Yazmaciyan, S. Zhumagali, W. Yan, Y. Gao, Z. Song, C. Li, S. Fu, B. Chen, A. ur Rehman, M. Babics, A. Razzaq, M. De Bastiani, T. G. Allen, U. Schwingenschlögl, Y. Yan, F. Laquai, E. H. Sargent and S. De Wolf, *Joule*, 2023, **8**, 224-240.
- 16 Z. Wang, L. Zeng, T. Zhu, H. Chen, B. Chen, D. J. Kubicki, A. Balvanz, C. Li, A. Maxwell, E. Ugur, R. Dos Reis, M. Cheng, G. Yang, B. Subedi, D. Luo, J. Hu, J. Wang, S. Teale, S. Mahesh, S. Wang, S. Hu, E. Jung, M. Wei, S. M. Park, L. Grater, E. Aydin, Z. Song, N. J. Podraza, Z. H. Lu, J. Huang, V. P. Dravid, S. De Wolf, Y. Yan, M. Gratzel, M. Kanatzidis and E. Sargent, *Nature*, 2023, **618**, 74-79.
- 17 Z.-W. Tao, T. Lu, X. Gao, M. U. Rothmann, Y. Jiang, Z.-Y. Qiang, H.-Q. Du, C. Guo, L.-H. Yang, C.-X. Wang, Y. Liu, Y.-B. Cheng and W. Li, *ACS Energy Lett.*, 2024, **9**, 1455-1465.

- 18 J. Thiesbrummel, S. Shah, E. Gutierrez-Partida, F. Zu, F. Peña-Camargo, S. Zeiske, J. Diekmann, F. Ye, K. P. Peters, K. O. Brinkmann, P. Caprioglio, A. Dasgupta, S. Seo, F. A. Adeleye, J. Warby, Q. Jeangros, F. Lang, S. Zhang, S. Albrecht, T. Riedl, A. Armin, D. Neher, N. Koch, Y. Wu, V. M. Le Corre, H. Snaith and M. Stolterfoht, *Nat. Energy*, 2024, **9**, 664-676.
- 19 H. Tsai, R. Asadpour, J. C. Blancon, C. C. Stoumpos, O. Durand, J. W. Strzalka, B. Chen, R. Verduzco, P. M. Ajayan, S. Tretiak, J. Even, M. A. Alam, M. G. Kanatzidis, W. Nie and A. D. Mohite, *Science*, 2018, **360**, 67-70.
- 20 F. Li, X. Deng, Z. Shi, S. Wu, Z. Zeng, D. Wang, Y. Li, F. Qi, Z. Zhang, Z. Yang, S.-H. Jang, F. R. Lin, S. W. Tsang, X.-K. Chen and A. K. Y. Jen, *Nat. Photon.*, 2023, **17**, 478-484.
- 21 Y. Zheng, Y. Li, R. Zhuang, X. Wu, C. Tian, A. Sun, C. Chen, Y. Guo, Y. Hua, K. Meng, K. Wu and C.-C. Chen, *Energy Environ. Sci.*, 2024, **17**, 1153-1162.
- 22 Q. Tan, Z. Li, G. Luo, X. Zhang, B. Che, G. Chen, H. Gao, D. He, G. Ma, J. Wang, J. Xiu, H. Yi, T. Chen and Z. He, *Nature*, 2023, **620**, 545-551.
- 23 X. Wang, Z. Ying, J. Zheng, X. Li, Z. Zhang, C. Xiao, Y. Chen, M. Wu, Z. Yang, J. Sun, J. R. Xu, J. Sheng, Y. Zeng, X. Yang, G. Xing and J. Ye, *Nat. Commun.*, 2023, **14**, 2166.
- 24 L. Qiao, T. Ye, T. Wang, W. Kong, R. Sun, L. Zhang, P. Wang, Z. Ge, Y. Peng, X. Zhang, M. Xu, X. Yan, J. Yang, X. Zhang, F. Zeng, L. Han and X. Yang, *Adv. Energy Mater.*, 2023, **14**, 2302983.
- 25 Y. Ou, H. Huang, H. Shi, Z. Li, Z. Chen, M. Mateen, Z. Lu, D. Chi and S. Huang, *Chem. Eng. J.*, 2023, **469**, 143860.
- 26 H. Luo, X. Zheng, W. Kong, Z. Liu, H. Li, J. Wen, R. Xia, H. Sun, P. Wu, Y. Wang, Y. Mo, X. Luo, Z. Huang, J. Hong, Z. Chu, X. Zhang, G. Yang, Y. Chen,

- Z. Feng, J. Gao and H. Tan, *ACS Energy Lett.*, 2023, **8**, 4993-5002.
- 27 M. Wu, X. Li, Z. Ying, Y. Chen, X. Wang, M. Zhang, S. Su, X. Guo, J. Sun, C. Shou, X. Yang and J. Ye, *Adv. Funct. Mater.*, 2023, **33**, 2304708.
- 28 W. Chai, L. Li, W. Zhu, D. Chen, L. Zhou, H. Xi, J. Zhang, C. Zhang and Y. Hao, *Research* 2023, **6**, 0196.
- 29 X. Li, Z. Ying, J. Zheng, X. Wang, Y. Chen, M. Wu, C. Xiao, J. Sun, C. Shou, Z. Yang, Y. Zeng, X. Yang and J. Ye, *Adv. Mater.*, 2023, **35**, 2211962.
- 30 A. Harter, S. Mariotti, L. Korte, R. Schlatmann, S. Albrecht and B. Stannowski, *Prog Photovolt Res Appl.*, 2023, **31**, 813-823.
- 31 W. Chi, S. K. Banerjee, K. G. D. I. Jayawardena, S. R. P. Silva and S. I. Seok, *ACS Energy Lett.*, 2023, **8**, 1535-1550.
- 32 Z. Ying, Z. Yang, J. Zheng, H. Wei, L. Chen, C. Xiao, J. Sun, C. Shou, G. Qin, J. Sheng, Y. Zeng, B. Yan, X. Yang and J. Ye, *Joule*, 2022, **6**, 2644-2661.
- 33 G. Yang, Z. Ni, Z. J. Yu, B. W. Larson, Z. Yu, B. Chen, A. Alasfour, X. Xiao, J. M. Luther, Z. C. Holman and J. Huang, *Nat. Photon.*, 2022, **16**, 588-594.
- 34 Q. Xu, B. Shi, Y. Li, L. Yan, W. Duan, Y. Li, R. Li, N. Ren, W. Han, J. Liu, Q. Huang, D. Zhang, H. Ren, S. Xu, C. Zhang, H. Zhuang, A. Lambertz, K. Ding, Y. Zhao and X. Zhang, *Adv. Energy Mater.*, 2022, **12**, 2202404.
- 35 D. Yu, M. Pan, G. Liu, X. Jiang, X. Wen, W. Li, S. Chen, W. Zhou, H. Wang, Y. Lu, M. Ma, Z. Zang, P. Cheng, Q. Ji, F. Zheng and Z. Ning, *Nat. Energy*, 2024, **9**, 298-307.
- 36 A. Maxwell, H. Chen, L. Grater, C. Li, S. Teale, J. Wang, L. Zeng, Z. Wang, S. M. Park, M. Vafaie, S. Sidhik, I. W. Metcalf, Y. Liu, A. D. Mohite, B. Chen and E. H. Sargent, *ACS Energy Lett.*, 2024, **9**, 520-527.
- 37 X. Zhou, H. Lai, T. Huang, C. Chen, Z. Xu, Y. Yang, S. Wu, X. Xiao, L. Chen, C.

- J. Brabec, Y. Mai and F. Guo, *ACS Energy Lett.*, 2023, **8**, 502-512.
- 38 S. Zhou, S. Fu, C. Wang, W. Meng, J. Zhou, Y. Zou, Q. Lin, L. Huang, W. Zhang, G. Zeng, D. Pu, H. Guan, C. Wang, K. Dong, H. Cui, S. Wang, T. Wang, G. Fang and W. Ke, *Nature*, 2023, **624**, 69-73.
- 39 J. Zhou, H. Qiu, T. Wen, Z. He, C. Zou, Y. Shi, L. Zhu, C. C. Chen, G. Liu, S. Yang, F. Liu and Z. Yang, *Adv. Energy Mater.*, 2023, **13**, 2300968.
- 40 Y. Zhao, C. Wang, T. Ma, L. Zhou, Z. Wu, H. Wang, C. Chen, Z. Yu, W. Sun, A. Wang, H. Huang, B. Zou, D. Zhao and X. Li, *Energy Environ. Sci.*, 2023, **16**, 2080.
- 41 Z. Yi, W. Wang, R. He, J. Zhu, W. Jiao, Y. Luo, Y. Xu, Y. Wang, Z. Zeng, K. Wei, J. Zhang, S. W. Tsang, C. Chen, W. Tang and D. Zhao, *Energy Environ. Sci.*, 2024, **17**, 202-209.
- 42 F. Yang, P. Tockhorn, A. Musiienko, F. Lang, D. Menzel, R. Macqueen, E. Kohnen, K. Xu, S. Mariotti, D. Mantione, L. Merten, A. Hinderhofer, B. Li, D. R. Wargulski, S. P. Harvey, J. Zhang, F. Scheler, S. Berwig, M. Ross, J. Thiesbrummel, A. Al-Ashouri, K. O. Brinkmann, T. Riedl, F. Schreiber, D. Abou-Ras, H. Snaith, D. Neher, L. Korte, M. Stolterfoht and S. Albrecht, *Adv. Mater.*, 2024, **36**, 230774.
- 43 Y. Wang, R. Lin, X. Wang, C. Liu, Y. Ahmed, Z. Huang, Z. Zhang, H. Li, M. Zhang, Y. Gao, H. Luo, P. Wu, H. Gao, X. Zheng, M. Li, Z. Liu, W. Kong, L. Li, K. Liu, M. I. Saidaminov, L. Zhang and H. Tan, *Nat. Commun.*, 2023, **14**, 1819.
- 44 W. Wang, X. Liu, J. Wang, C. Chen, J. Yu, D. Zhao and W. Tang, *Adv. Energy Mater.*, 2023, **13**, 2300694.
- 45 C. Liu, R. Lin, Y. Wang, H. Gao, P. Wu, H. Luo, X. Zheng, B. Tang, Z. Huang, H. Sun, S. Zhao, Y. Guo, J. Wen, F. Fan and H. Tan, *Angew. Chem. Int. Ed.*, 2023, **62**, e202313374.

- 46 R. Lin, Y. Wang, Q. Lu, B. Tang, J. Li, H. Gao, Y. Gao, H. Li, C. Ding, J. Wen, P. Wu, C. Liu, S. Zhao, K. Xiao, Z. Liu, C. Ma, Y. Deng, L. Li, F. Fan and H. Tan, *Nature*, 2023, **620**, 994-1000.
- 47 T. Li, J. Xu, R. Lin, S. Teale, H. Li, Z. Liu, C. Duan, Q. Zhao, K. Xiao, P. Wu, B. Chen, S. Jiang, S. Xiong, H. Luo, S. Wan, L. Li, Q. Bao, Y. Tian, X. Gao, J. Xie, E. H. Sargent and H. Tan, *Nat. Energy*, 2023, **8**, 610-620.
- 48 S. Wu, Y. Yan, J. Yin, K. Jiang, F. Li, Z. Zeng, S.-W. Tsang and A. K. Y. Jen, *Nat. Energy*, 2024, **9**, 411-421.
- 49 S. Qin, C. Lu, Z. Jia, Y. Wang, S. Li, W. Lai, P. Shi, R. Wang, C. Zhu, J. Du, J. Zhang, L. Meng and Y. Li, *Adv. Mater.*, 2022, **34**, 2108829.
- 50 L. Liu, H. Xiao, K. Jin, Z. Xiao, X. Du, K. Yan, F. Hao, Q. Bao, C. Yi, F. Liu, W. Wang, C. Zuo and L. Ding, *Nanomicro Lett.*, 2022, **15**, 23.
- 51 X. Gu, X. Lai, Y. Zhang, T. Wang, W. L. Tan, C. R. McNeill, Q. Liu, P. Sonar, F. He, W. Li, C. Shan and A. K. K. Kyaw, *Adv. Sci.*, 2022, **9**, 2200445.
- 52 W. Chen, Y. Zhu, J. Xiu, G. Chen, H. Liang, S. Liu, H. Xue, E. Birgersson, J. W. Ho, X. Qin, J. Lin, R. Ma, T. Liu, Y. He, A. M.-C. Ng, X. Guo, Z. He, H. Yan, A. B. Djurišić and Y. Hou, *Nat. Energy*, 2022, **7**, 229-237.
- 53 K. O. Brinkmann, T. Becker, F. Zimmermann, C. Kreusel, T. Gahlmann, M. Theisen, T. Haeger, S. Olthof, C. Tückmantel, M. Günster, T. Maschwitz, F. Göbelmann, C. Koch, D. Hertel, P. Caprioglio, F. Peña-Camargo, L. Perdigón-Toro, A. Al-Ashouri, L. Merten, A. Hinderhofer, L. Gomell, S. Zhang, F. Schreiber, S. Albrecht, K. Meerholz, D. Neher, M. Stolterfoht and T. Riedl, *Nature*, 2022, **604**, 280-286.
- 54 X. Wu, Y. Liu, F. Qi, F. Lin, H. Fu, K. Jiang, S. Wu, L. Bi, D. Wang, F. Xu, A. K. Y. Jen and Z. Zhu, *J. Mater. Chem. A*, 2021, **9**, 19778-19787.

- 55 Z. Zhang, W. Chen, X. Jiang, J. Cao, H. Yang, H. Chen, F. Yang, Y. Shen, H. Yang, Q. Cheng, X. Chen, X. Tang, S. Kang, X.-m. Ou, C. J. Brabec, Y. Li and Y. Li, *Nat. Energy*, 2024, **9**, 592-601.
- 56 N. Shrivastav, S. Kashyap, J. Madan, A. K. Al-Mousoi, M. K. A. Mohammed, M. K. Hossain, R. Pandey and J. Ramanujam, *Energy Fuels*, 2023, **37**, 3083-3090.
- 57 M. Nakamura, C. C. Lin, C. Nishiyama, K. Tada, T. Bessho and H. Segawa, *ACS Appl. Energy Mater.*, 2022, **5**, 8103-8111.
- 58 D. Wang, H. Guo, X. Wu, X. Deng, F. Li, Z. Li, F. Lin, Z. Zhu, Y. Zhang, B. Xu and A. K. Y. Jen, *Adv. Funct. Mater.*, 2022, **32**, 2107359.
- 59 C. Chen, J. Liang, J. Zhang, X. Liu, X. Yin, H. Cui, H. Wang, C. Wang, Z. Li, J. Gong, Q. Lin, W. Ke, C. Tao, B. Da, Z. Ding, X. Xiao and G. Fang, *Nano Energy*, 2021, **90**, 106608.
- 60 M. Jošt, E. Köhnen, A. Al-Ashouri, T. Bertram, Š. Tomšič, A. Magomedov, E. Kasparavicius, T. Kodalle, B. Lipovšek, V. Getautis, R. Schlatmann, C. A. Kaufmann, S. Albrecht and M. Topič, *ACS Energy Lett.*, 2022, **7**, 1298-1307.
- 61 L. Tang, X. Wang, X. Liu, J. Zhang, S. Wang, Y. Zhao, J. Gong, J. Li and X. Xiao, *Adv. Sci.*, 2022, **9**, 2201768.
- 62 D. H. Kim, C. P. Muzzillo, J. Tong, A. F. Palmstrom, B. W. Larson, C. Choi, S. P. Harvey, S. Glynn, J. B. Whitaker, F. Zhang, Z. Li, H. Lu, M. F. A. M. van Hest, J. J. Berry, L. M. Mansfield, Y. Huang, Y. Yan and K. Zhu, *Joule*, 2019, **3**, 1734-1745.
- 63 A. Al-Ashouri, A. Magomedov, M. Roß, M. Jošt, M. Talaikis, G. Chistiakova, T. Bertram, J. A. Márquez, E. Köhnen, E. Kasparavičius, S. Levencenco, L. Gil-Escríg, C. J. Hages, R. Schlatmann, B. Rech, T. Malinauskas, T. Unold, C. A. Kaufmann, L. Korte, G. Niaura, V. Getautis and S. Albrecht, *Energy Environ. Sci.*, 2019, **12**,

- 3356-3369.
- 64 Q. Han, Y.-T. Hsieh, L. Meng, J.-L. Wu, P. Sun, E.-P. Yao, S.-Y. Chang, S.-H. Bae, T. Kato, V. Bermudez, Y. Yang, *Science*, 2018, **361**, 904-908.
- 65 F. Li, D. Wu, L. Shang, R. Xia, H. Zhang, Z. Huang, J. Gong, L. Mao, H. Zhang, Y. Sun, T. Yang, X. Sun, Z. Feng and M. Liu, *Adv. Mater.*, 2024, **36**, 2311595.
- 66 Y. J. Choi, S. Y. Lim, J. H. Park, S. G. Ji and J. Y. Kim, *ACS Energy Lett.*, 2023, **8**, 3141-3146.
- 67 J. Zheng, G. Wang, W. Duan, M. A. Mahmud, H. Yi, C. Xu, A. Lambertz, S. Bremner, K. Ding, S. Huang and A. W. Y. Ho-Baillie, *ACS Energy Lett.*, 2022, **7**, 3003-3005.
- 68 J. Werner, F. Sahli, F. Fu, J. J. Diaz Leon, A. Walter, B. A. Kamino, B. Niesen, S. Nicolay, Q. Jeangros and C. Ballif, *ACS Energy Lett.*, 2018, **3**, 2052-2058.
- 69 H. Hu, S. X. An, Y. Li, S. Orooji, R. Singh, F. Schackmar, F. Laufer, Q. Jin, T. Feeney, A. Diercks, F. Gota, S. Moghadamzadeh, T. Pan, M. Rienäcker, R. Peibst, B. A. Nejand and U. W. Paetzold, *Energy Environ. Sci.*, 2024, **17**, 2800-2814.
- 70 S. Liu, Y. Lu, C. Yu, J. Li, R. Luo, R. Guo, H. Liang, X. Jia, X. Guo, Y.-D. Wang, Q. Zhou, X. Wang, S. Yang, M. Sui, P. Müller-Buschbaum and Y. Hou, *Nature*, 2024, **628**, 306-312.
- 71 J. Wang, L. Zeng, D. Zhang, A. Maxwell, H. Chen, K. Datta, A. Caiazzo, W. H. M. Remmerswaal, N. R. M. Schipper, Z. Chen, K. Ho, A. Dasgupta, G. Kusch, R. Ollearo, L. Bellini, S. Hu, Z. Wang, C. Li, S. Teale, L. Grater, B. Chen, M. M. Wienk, R. A. Oliver, H. J. Snaith, R. A. J. Janssen and E. H. Sargent, *Nat. Energy*, 2024, **9**, 70-80.
- 72 J. Wang, V. Zardetto, K. Datta, D. Zhang, M. M. Wienk and R. A. J. Janssen, *Nat. Commun.*, 2020, **11**, 5254.

- 73 D. P. McMeekin, S. Mahesh, N. K. Noel, M. T. Klug, J. Lim, J. H. Warby, J. M. Ball, L. M. Herz, M. B. Johnston and H. J. Snaith, *Joule*, 2019, **3**, 387-401.
- 74 F. H. Isikgor, T. Maksudov, X. Chang, B. Adilbekova, Z. Ling, W. T. Hadmojo, Y. Lin and T. D. Anthopoulos, *ACS Energy Lett.*, 2022, **7**, 4469-4471.
- 75 Z. Yang, A. Surrente, K. Galkowski, A. Miyata, O. Portugall, R. J. Sutton, A. A. Haghimirad, H. J. Snaith, D. K. Maude, P. Plochocka and R. J. Nicholas, *ACS Energy Lett.*, 2017, **2**, 1621-1627.